The corrosion behavior of mild steel in soft alkaline cooling water in relation to phosphorus-free corrosion inhibitors

Master Thesis

Wyona Boers

The corrosion behavior of mild steel in soft alkaline cooling water in relation to phosphorus-free corrosion inhibitors

By: Wyona Boers

For the degree of: Master of Science in Civil Engineering

To be defended publicly on: Tuesday August 21, 2018 at 12:00 PM

Graduation committee:

Dr. ir. H. Spanjers	Delft University of Technology Section Sanitary Engineering
Dr. ir. D.H. Moed	Evides Industrie Water
Dr. ir. S.G.J. Heijman	Delft University of Technology Section Sanitary Engineering
Prof. dr. ir. J.B. van Lier	Delft University of Technology Section Sanitary Engineering
Prof. dr. ir. J.M.C. Mol	Delft University of Technology Section Corrosion Technology and Electrochemistry

Delft University of Technology
Faculty of Civil Engineering and Geosciences
Department of Water Management
Section Sanitary Engineering

TU Delft

Evides industriewater

Preface

This report is the result of my graduation research for the MSc track Water Management at the Delft University of Technology. Looking back, I can affirm that studying at the TU Delft has taught me a lot, opened many doors and led to invaluable experiences. Finishing my MSc studies would not have been possible without the support that I received.

Firstly, I would like to thank Luuk Rietveld for encouraging me to pursue my studies in the section of Sanitary Engineering. Secondly, regarding my graduation work, I would like to thank several people that have been part of the process. Henri Spanjers, you introduced me in the world of industry water and remained a patient supervisor despite the time I took to finish the work. David, thank you for enabling the partnership with Evides Industriewater. It was absolutely interesting to assist you with the pilot cooling tower in Terneuzen. Both David and Ingrid, thank you for your support and for continuing to keep me updated about the second pilot. Furthermore, Jules van Lier and Bas Heijman, thank you for your lectures and for being part of my graduation committee.

Additionally, I'm very grateful to Arjan Mol, you welcomed me in the Corrosion Technology and Electrochemistry group. Mats and Joost, thank you for guiding me in the corrosion labs, helping out with the potentiostats and making the lab life more sociable together with the other Rusty People. The Waterlab and the faculty of Mechanical, Maritime and Materials Engineering, with all the workshops and lab facilities, have been a true play ground to me. This can be credited to the support of the (lab) technicians, Mohammed, Armand, Agnieszka, Sander and Wim.

At last, I am thankful for my family and friends, who provided the distraction and the help that I was seeking for. Charlotte, thank you for showing up when needed most and for encouraging me to take the programming one level up. Maurits, I owe you great gratitude, I feel privileged with your genuine support and your eagerness to understand my work.

Soli Deo gloria.

Wyona Boers
Delft, August 2018

Abstract

Water as a coolant for industrial products or processes is widely used. Efficient operation of Open Recirculating Cooling Water Systems (ORCWS) relies on controlled cooling water conditioning programs that prevent corrosion, fouling, scaling and microbial growth. Water intensive industries feel greater pressure to decrease their water demand as water resources become increasingly stressed and discharge restrictions become more stringent. Pre-treating the cooling water before it enters the recirculation stream provides the opportunity to reduce the water demand and to seek for alternative chemicals, preferably less complex and with a lower stress on the environment. Soft alkaline cooling water (SACW) might be a good alternative for the conventional water and chemicals intensive ORCWS operation. However, this type of water requires complete reevaluation of the conditioning programs. Therefore, this research focused on the corrosion processes in SACW and a beginning was made in evaluating non-toxic and phosphorus-free corrosion inhibitors.

The research comprised the production of synthetic cooling water (SCW) and the evaluation of corrosion of mild steel in this type of water, with and without inhibitors. The selected corrosion inhibitors were NovoTraqua® without phosphorus (NT0) and sodium silicate (Si200). PHREEQC simulation were used to validate the SCW composition. A desk study was carried out to evaluate the applicability of corrosion indices. The average corrosion rate and inhibition efficiency were determined by mass loss tests of mild steel specimens with an immersion time of up to 4 weeks. The development of passivity was followed by open circuit potential (OCP) measurements. The pitting susceptibility was tested using cyclic potentiodynamic anodic polarization (CPP) measurements. 3D digital microscopy, SEM/EDS and XRD were used to evaluate the surface morphology and the composition of the top layer.

The calculations for the SCW resembled PHREEQC simulations. A natural pH of 9.1 was reached based on the carbonate equilibrium. Small corrections in the $NaHCO_3$ and Na_2CO_3 dosage were applied to increase the pH to the desired pH 9.4. The existing corrosion indices are not suitable to be applied to SCW. The immersion of mild steel with a roughness of 30µm in SCW resulted in uniform corrosion. The addition of NT0 or Si200 to the SCW resulted in the inhibition of uniform corrosion but no complete protection against localized corrosion was realized. Si200 was the best performing inhibitor. The immersion of mild steel with a 7µm roughness in SCW resulted in natural passivation by the formation of a Fe_2O_3 oxide layer. The SCW did not have the ability to immediately repassivate the specimens after localized breakdown of the protecting passivating layer. The addition of NT0 or Si200 reduced the aggressiveness of the environments at the pits but did not accomplish complete repassivation.

Lab experiments with SCW can provide initial insights in the behavior of mild steel and can contribute to the decision making in more cost intensive research on alternative operation of ORCWS. The experiments should be extended by testing the behavior and inhibition of corrosion at different temperatures, inhibitor concentrations, phosphonate concentrations and different

cycles of concentration. Better understanding of the protection mechanisms would be obtained when more advanced techniques like Fourier Transform Infrared Spectroscopy (FTIR) and Electrochemical Impedance Spectroscopy (EIS) are used. Although cooling water corrosion inhibition by means of silica is a mature research topic, it is recommended to proceed with research on silica as a corrosion inhibitor in the specific conditions of SACW.

Contents

List of Figures

List of Tables

1 Introduction

1.1 Background and Problem description

Water as a coolant for industrial products or processes is widely used considering its availability in most industrialized areas, its nontoxicity, its relatively high heat capacity, and its thermal conductivity. The heat from the hot process fluids is transferred to the cooling water in a heat exchanger and carried away by the cooling water. The performance of a cooling water system (CWS) is critical for the production process. Failure of the cooling system can result in decreased heat transfer, economic losses due to unscheduled shut downs, and failure of the production equipment.

The concentration of the dissolved and suspended solids, and the contamination of the cooling water through interaction with the atmosphere, cause highly undesired processes for Open Recirculating Cooling Water Systems (ORCWS). Corrosion of metal, formation of scale, fouling of the system, and bacterial growth are all undesired processes, that also influence and intensify each other. This mutual interaction is schematized in Figure 1, and an example would be that when insoluble corrosion or scale products aggregate and settle, it results in fouling and occluded areas, which again results in growth sites for microbiology and under deposit corrosion. ORCWS efficient operation depends on controlled cooling water conditioning programs to counteract these processes that occur simultaneously. Conventional conditioning programs rely on a tailored mixture of corrosion, scaling and fouling inhibitors. Toxic chemicals, such as chromate, were commonly used in corrosion inhibitors for cooling water conditioning programs until prohibited by legislation. Current prevailing alternatives for those toxic inhibitors are phosphorus containing inhibitors. [1,2]

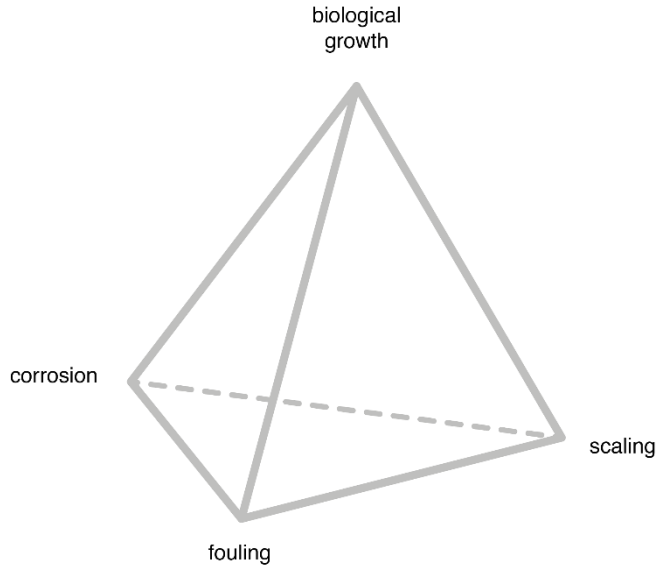

Figure 1: Tetrahedron of undesired interacting processes in ORCWS.

A robust and reliable operation of the ORCWS is crucial, and opportunities to reduce the operational costs and the environmental impact are explored. Water intensive industries feel greater pressure to decrease their water demand as water resources become increasingly stressed and discharge restrictions become more stringent. The cooling towers and infrastructure may often not have reached their end of life, therefore redesigning the cooling water conditioning can provide possible solutions. Conditioning the cooling water before it enters the recirculation stream provides the opportunity to reduce the water demand and to seek for alternative inhibitors, preferably less complex and with a lower stress on the environment.

One of the options to condition the water before it enters the ORCWS is to apply complete softening. Softening is about the removal of bivalent cations, calcium and magnesium ions in particular. By applying softening as a pretreatment step, the risk of scaling of the ORCWS is reduced and the opportunity to operate at higher concentration ratios is established. Besides, the recirculating cooling water in an ORCWS develops a natural high pH due to the gas exchange with atmosphere. Common practice, to reduce the risk of scaling, is to correct the pH to a value in the range of pH 7 to pH 8.5 with acids or to apply an All-Organic inhibition program that contains phosphonates and which is effective at an elevated pH. So without the presence of scale forming ions, it would be possible to operate the ORCWS at a higher concentration ratio and at a naturally established pH, resulting in a decrease of the water demand, of the loss of inhibitors, and of the need for pH correcting acids or the need for complex phosphorus containing inhibition programs.

Although operating a ORCWS with soft water mitigates the risk of scaling, other undesired processes, like corrosion, will still occur and require inhibition. Prevailing corrosion inhibitors for soft alkaline cooling water (SACW) are zinc, molybdate, phosphonates and organic phosphates [1]. However, non-disrupting inhibitors are characterized by non-toxicity and macro nutrient limitation, which is not applicable to the corrosion inhibitors just mentioned. Therefore, sustainable operation of ORCWS with SACW requires a reevaluation of the suitable corrosion inhibitors.

Limiting phosphorus has positive consequences for the water quality. Firstly, high phosphorus concentrations in the reject water disturb the environment by causing eutrophication. The maximum phosphorus concentration is restricted by legislation and is expected to become even lower by law in the future. Consequently, the reject water requires advanced treatment before being discharged to surface waters. Secondly, phosphorus is also a macronutrient and vital for the undesired microbial growth in the ORCWS. The microbial growth is not only regulated by organic carbon but also by the phosphorus and nitrogen concentration [3]. New technologies, like BioPhree® [4], are being developed to remove phosphorus efficiently from pre-treated water. The combination of a high pH and limited phosphorus content may be an alternative for the usage of biocides to reduce the microbial activity in ORCWS.

According to a desk study executed by KWR Watercycle Research Institute (KWR) [5], it is expected to be cost and environmentally advantageous to apply complete softening before the water enters the recirculation stream of the ORCWS. Operating ORCWS with soft water is not a

new phenomenon to the industry but corrosion remains a complex process that is not without ambiguity and requires research [6]. Water engineers are often confident in assessing the scaling potential, for which indices and rules of thumb have been developed. Attempts have been made to come up with corrosion indexes but those are limited in their usage range [5,7–10].

Corrosion research can focus on a great variety of metals and alloys. A widespread and economical construction material for cooling water systems is mild or low-carbon steel. Corrosion research on mild steel for ORCWS has been performed in soft water, albeit at (near) neutral pH, and in more alkaline water, but which contained calcium and magnesium ions [11–17]. Research focusing on corrosion in concrete or in boiler systems does utilize soft alkaline solutions. Nevertheless, this research generally excludes the presence of oxygen [18]. A respectable amount of corrosion research on construction metals in aqueous environments is related to the oil and gas industry and focusses on very saline conditions, on acidic conditions, and on carbon dioxide corrosion [19,20]. Nor do those conditions prevail in ORCWS. So more knowledge is to be gained on the corrosion behavior of mild steel in SACW to accomplish more sustainable operation of ORCWS, as was recommended by KWR [5].

1.2 Objective and Research Questions

This thesis focusses on the corrosion processes in SACW and a beginning is made in evaluating non-toxic and phosphorus-free corrosion inhibitors. The main goal of this thesis is:

“To gain understanding of the corrosion behavior of mild steel in soft alkaline cooling water, to test the effect of different corrosion inhibitors on the corrosion behavior, and to explore phosphorus-free corrosion inhibitors for this type of cooling water”.

This goal is reached in such a way that the results contribute to the decision making and understanding of other (pilot scale) research projects that support the operation of ORCWS without the addition of toxic or phosphorus containing inhibitors.

Exploring the different types of corrosion assessment techniques and selecting the appropriate tests for this thesis is key. This results in the first research question:

A. How can the corrosion behavior of mild steel in soft alkaline cooling water be evaluated?

The selected tests and test conditions are first of all used to discuss the effect of only SACW on the corrosion of mild steel before the effect of different inhibitors is tested. Therefore, the following two questions are posed:

B. What is the effect of soft alkaline cooling water on the corrosion behavior of mild steel?
C. How do different non-toxic corrosion inhibitors affect the corrosion behavior of mild steel in soft alkaline cooling water?

It is expected from the answers to the previous questions that a corrosion inhibitor is required to establish a sufficient protective layer on the surface of mild steel. The next step is to evaluate if the corrosion inhibitor can be protective without the presence of additional phosphorus.

D. How do different concentrations of phosphorus in the corrosion inhibitor affect the corrosion behavior of mild steel in soft alkaline cooling water?

1.3 Research approach and Report Outline

The report provides first of all, in Chapter 2, some theoretical background on CWS, on corrosion in aqueous environments, and on different techniques and methods that can be applied to evaluate corrosion. This is based on literature review. Chapter 3, 4, and 5 each cover a different experimental phase. Therefore, each of these three chapters is split up into ‘materials and methods’ and ‘results and discussion’. Chapter 3 describes what kind of cooling water is used for the experiments and what the characteristics are. This water is used for the actual corrosion experiments that are described in Chapter 4 and 5. Chapter 4 evaluates corrosion in different solutions based on mass loss experiments, while Chapter 5 evaluates corrosion in different solutions based on potential and current density measurements. Finally, the research questions presented in the previous section are answered in Chapter 6 and the recommendations that arose from the research are provided in Chapter 7.

The relevance of this research is directed at open recirculating cooling water systems, which will be for remainder of thesis referred to as cooling water systems or CWS.

2 Theoretical background

2.1 Open recirculating cooling systems

In CWS, the heat of the cooling water is released through evaporation. As a result, the dissolved and suspended solids in the cooling water become more concentrated. The water that leaves the cooling tower by evaporation and other losses is replenished with unconcentrated water, called *makeup water*, to avoid further concentration increase. The solids concentration in the cooling water is regulated by controlled discharge of this water as *blowdown*. The different water flows and losses are illustrated in Figure 2. The ratio of an ion concentration in the blowdown (C_{bd}) to the concentration of the same ion in the makeup water (C_{mu}) is defined as *cycles of concentration* (COC) or the concentration ratio, as in Equation (2.1).

$$COC = \frac{C_{bd}}{C_{mu}} \tag{2.1}$$

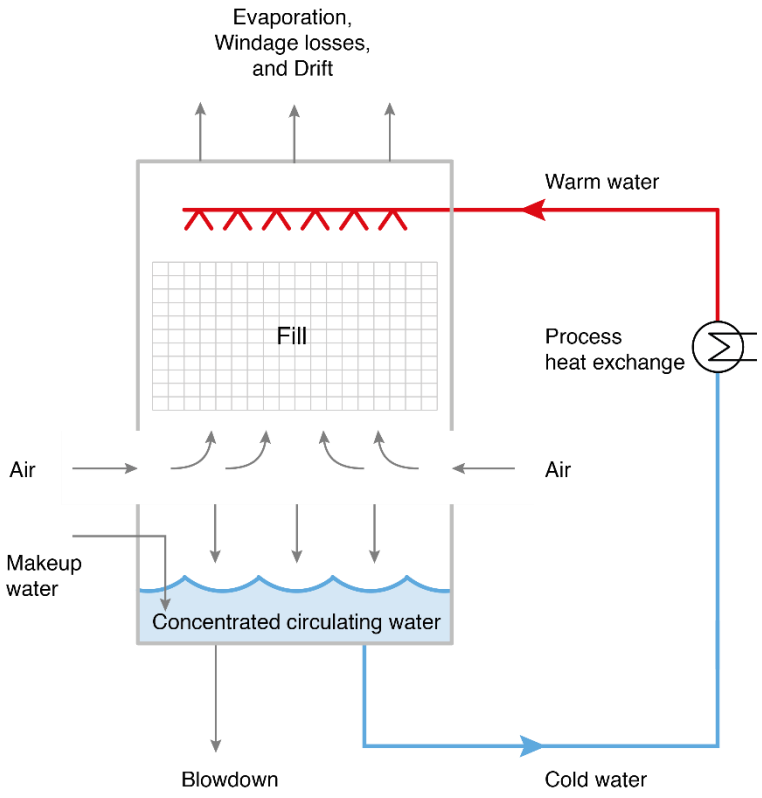

Figure 2: Schematization of an Open Recirculating Cooling Water System.

The blowdown rate (BD) and the makeup rate (MU) depend on the evaporation rate (E) and the desired COC, as is given in Equation (2.2) and (2.3) and illustrated in Figure 3. Operating at a higher COC reduces the blowdown rate. The makeup rate is asymptotically limited by the evaporation rate, because the evaporation rate is dependent on the conditions of the system and the atmosphere.

$$BD = \frac{E}{(COC - 1)} \tag{2.2}$$

$$MU = \frac{E \cdot COC}{(COC - 1)} \tag{2.3}$$

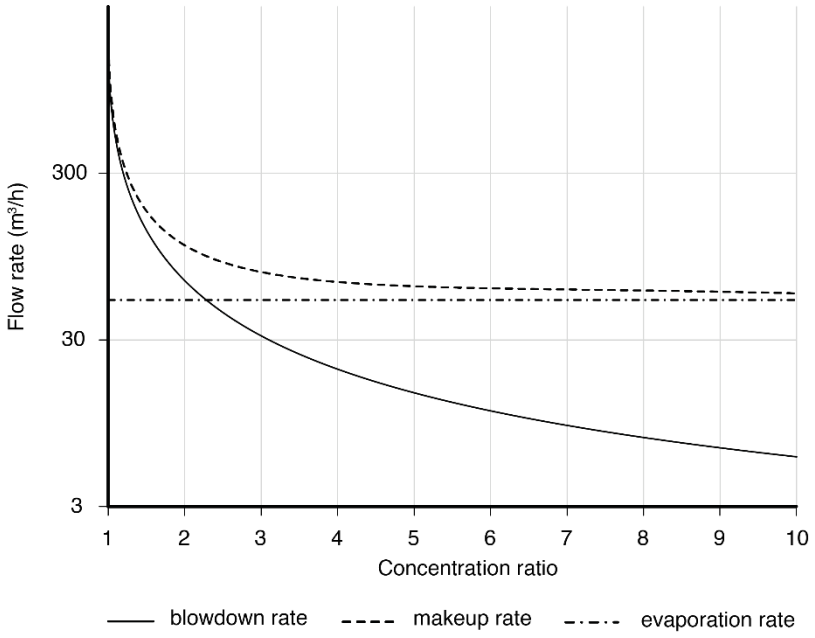

Figure 3: Makeup rate and blowdown as a function of COC.

The concentration of ions and inhibitors in a CWS is carefully monitored and regulated. The *holding time index* (HTI) is defined as the time required for the concentration of an ion to dilute to half of its original concentration within the systems volume (V). It is calculated with Equation (2.4).

$$HTI = \frac{\ln(2) \cdot V}{BD} \tag{2.4}$$

Increasing the COC, when initially operating the CWS at a COC up to five, will reduce the water demand. Increasing the COC above six has no effect on the water demand but it does still reduce the volume of the waste stream and the amount of chemicals that is lost.

2.2 Corrosion in aqueous environments

2.2.1 Thermodynamics and kinetics of iron corrosion

The deterioration of metal in an aqueous environment in case of corrosion is an electrochemical process where the metal returns to its natural oxide state. Corrosion occurs if an *electrochemical corrosion cell* is established. This cell comprises an anode, a cathode, a ionic current path, and an electronic path, as is shown schematically in Figure 4. The *anode* generates electrons and positively charged metal ions in an *oxidation reaction*. The *cathode* consumes electrons in a *reduction reaction*.

The anodic oxidation reaction of a metal in general:

$$M \rightarrow M^{n+} + ne^{-} \tag{2.5}$$

The cathodic reduction reaction in natural waters of neutral or alkaline pH, is dominated by the oxygen reduction reaction:

$$O_2 + 2H_2O + 4e^{-} \rightarrow 4OH^{-} \qquad E_0 = +\ 0.40\ \text{V SHE} \tag{2.6}$$

The ionic current path is established in a conducting electrolyte. The electronic path transfers the electrons from the anode to the cathode, establishing an electric current. The driving force of the electrochemical corrosion reaction is the *electrical-potential difference* between the anode and the cathode, and causes current to flow between the anode and the cathode.

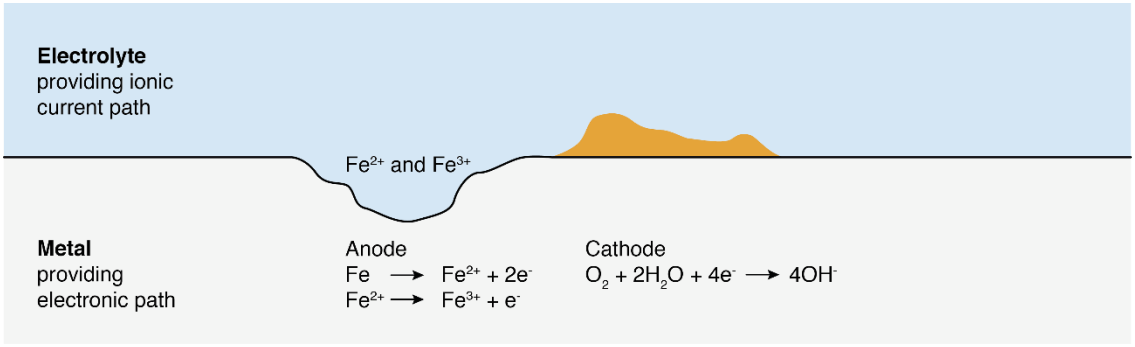

Figure 4: Schematic corrosion cell of iron in an aqueous environment.

The electrochemical processes can be displayed in a thermodynamic framework based on equilibrium equations. Based on these thermodynamic equilibria, the electrode potential can be plotted in a graph against a chosen factor, pH or temperature for example. The graph will show the conditions of thermodynamic stability based on the lowest free-energy state for the reactions considered. Figure 5 is a simplified *potential-pH equilibrium diagram* for iron-water from Pourbaix [21].

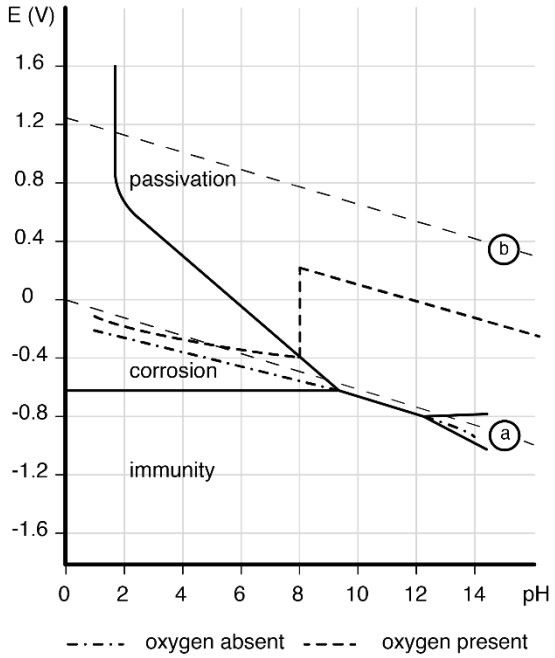

Figure 5 Simplified theoretical potential-pH diagrams for iron in water, with the experimental equilibrium potentials in the absence and in the presence of oxygen (based on diagrams in [21]).

Three type of domains or particular types of stability can be distinguished, namely corrosion (stability of a dissolved species), *immunity* (stability of the metal), and *passivity* (stability of solid oxides or salts) [22]. The dashed lines 'a' and 'b' indicate the stability domain of water, which is defined by the electrochemical reactions of hydrogen evolution and oxygen reduction according to Equation (2.7) and (2.8).

$$2H^+ + 2e^- \rightarrow H_2 \qquad E_0 = 0.0 \text{ V SHE} \qquad (2.7)$$

$$O_2 + 4H^+ + 4e^- \rightarrow 2H_2O \qquad E_0 = +1.23 \text{ V SHE} \qquad (2.8)$$

Series of experiments have been performed to examine the behavior of iron in various aqueous solutions and under various conditions of pH and electrode potential to determine domains of corrosion, immunity and passivation, and to compare this with the theoretically established diagrams [21]. Figure 5 represents the results from experiments by Pourbaix [21] of iron in solutions free from oxygen and in solutions saturated with oxygen at atmospheric pressure. The presence of oxygen increased the potential of iron. The potential of iron is even raised to the passivation domain at pHs above 8. Evans [23,24] had already proven that iron, in a solution that contains oxygen, is passivated by an oxide film and that differential aeration increases the corrosion rate in the non-aerated regions. Mayne and Pryor [25,26] reported that the electrode potential of iron increases in the presence of oxygen in the solution. In an aerated solution, a thin film of Fe_2O_3 is formed, which institutes the development of positive potentials. It is believed that this film eventually becomes impervious to oxygen and to ions, establishing protection against corrosion.

Thermodynamic calculations or potential-pH diagrams are useful as a first study of the expected stability domain, but do not provide information on the reactions rates or the transformation process from iron to an iron oxide. The two common oxidation states for iron are Fe(II) and Fe(III), ferrous and ferric iron, respectively. Ferric iron is the stable oxidation state in aqueous solutions in equilibrium with the atmosphere.

Before stable oxide products are formed, the transformation of the iron in the steel surface undertakes different electrochemical reactions. The Fe^{2+} ion is the initial product created by the anodic dissolution reaction of steel:

$$Fe \rightarrow Fe^{2+} + 2e^{-} \qquad E_0 = \text{-0.44 V SHE} \qquad (2.9)$$

which can either form simple salts with most anions or it forms the first hydroxide, $Fe(OH)_2$ (ferrous hydroxide). The reaction in Equation (2.9) is complemented by the cathodic reduction reaction of oxygen given in Equation (2.8), resulting overall reaction:

$$2Fe + O_2 + 2H_2O \rightarrow 2Fe(OH)_2 \qquad (2.10)$$

$Fe(OH)_2$ has a low solubility product, as is given in Equation (2.11). Therefore, $Fe(OH)_2$ is formed close to the metal surface and deposited on the surface. Ferrous hydroxide is however unstable in a solution that is in equilibrium with the atmosphere and is therefore further oxidized to form $Fe_2O_3 \cdot nH_2O$ (hydrous iron(III) oxide), FeO(OH) (iron(III) oxide hydroxide), Fe_2O_3 (anhydrous iron(III)oxide) or Fe_3O_4 (magnetite). Fe_3O_4 is stable in oxygen limited environments. The reaction to form $Fe_2O_3 \cdot nH_2O$ is given in Equation (2.12).

$$K_s = (a_{Fe^{2+}})(a_{OH^-})^2 = 1.64 \times 10^{-14} \qquad \text{at } 18°C \qquad (2.11)$$

$$2Fe^{II}(OH)_2 + 2OH^- = Fe^{III}{}_2O_3 \cdot H_2O + 2H_2O + 2e^- \qquad (2.12)$$

FeO(OH), Fe_2O_3 and Fe_3O_4 can form coherent adherent layers on the metal that passivate the metal by inhibiting the transport of reacting species between the metal and its environment, called a *passivating layer* or *passive film*. Cohen [27] proposed several models of passive film on iron and Strehblow [28,29] confirmed that for iron an inner Fe_3O_4 film is followed by Fe_2O_3 with the possibility of FeO(OH) on top in alkaline solutions.

For the formation of a protective passivating layer it is key that the ferrous ions precipitate immediately and rapidly at the surface and get further oxidized to protective ferric compounds. This requires a sufficient supply of oxygen. This supply of oxygen to the metal surface layer is slow unless the velocity of water relative to the metal surface is sufficiently high. The corrosion of steel in air-saturated water is under diffusion control of dissolved oxygen because of the limiting concentration and diffusion coefficient of oxygen, and because of the rapid corrosion reaction when oxygen reaches the steel surface. The reaction rate of the oxygen reduction reaction is strongly pH dependent and is highest in an alkaline environment. The unavailability of dissolved oxygen due to limiting diffusion can result in unprotective Fe^{2+} products.

2.2.2 Localized corrosion

Two types of localized corrosion are pitting corrosion and crevice corrosion. *Pitting* is a highly localized form of attack that often results in small anodic sites where holes are created that can penetrate deep into the metal. Failure of the passive film or the formation of concentration cells under a deposit can result in pitting. Pitting can be induced by halide ions, most commonly by the Cl^- ion. Its unpredictable behavior can cause sudden failure of the metal. *Crevice corrosion* occurs in crevices where the solution is often stagnant. Figure 6 provides an overview of the possible pit shapes.

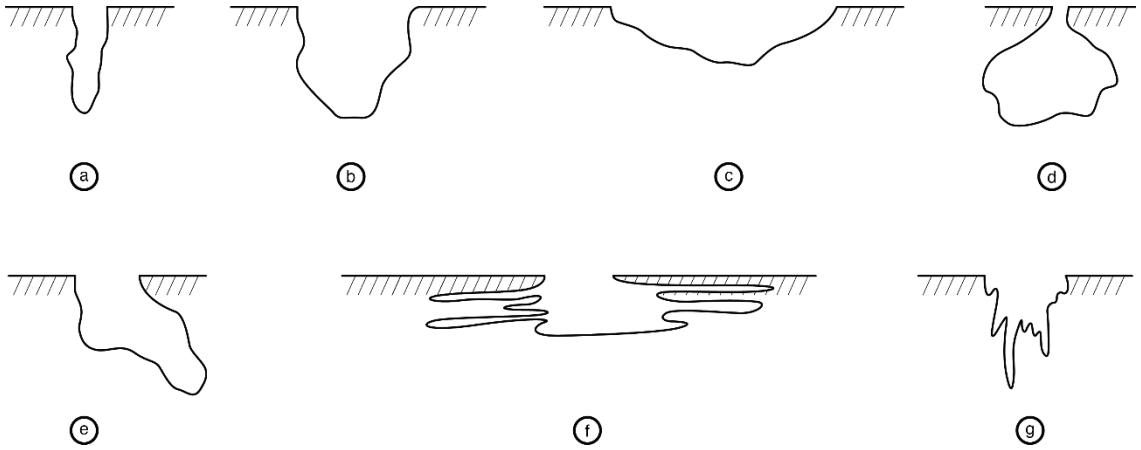

Figure 6: Variation in the cross-sectional shape of pits. (a) Narrow and deep. (b) Elliptical. (c) Wide and shallow. (d) Subsurface. (e) Undercutting. (f) Shapes determined by microstructural orientation. [30]

2.2.3 Water parameters affecting corrosion

Although corrosion of mild steel in aerated water proceeds by the action of dissolved oxygen, the rate of the reaction is affected by multiple parameters. The water quality parameters that especially affect the corrosivity of water are pH, DO, hardness, alkalinity, TDS, natural organic matter concentration, iron concentration, silica concentration and Cl^-, and SO_4^{2-} ions [1,31,32]. Cl^-, and SO_4^{2-} are aggressive ions that interfere with the protective film and enhance localized corrosion. Insoluble ferric ions (Fe^{3+}) can form porous layers of rust resulting in fouling. Silicon dioxide (SiO_2), or *silica*, can form a tenacious silica scale that is hard to remove from the system. Organic matter can foul the system, enhance the growth microbiology and cause under deposit corrosion.

Waters from which Ca^{2+} and Mg^{2+} have been removed result in different corrosion behavior than waters that still contain hardness. Normally, water that has sufficient hardness and alkalinity will result in $CaCO_3$ precipitation at the cathodes. This layer of scale acts as a barrier against the diffusion of oxygen and against electron transfer. On the other hand, it has been established that bicarbonate in the absence of Ca^{2+} can act as an inhibitor to corrosion of steel, as contrasted to the accelerative effect of Cl^- and SO_4^{2-} [32–34]. Indices have been developed that use the parameters

mentioned at the beginning of this section to provide information on the scaling and corrosion tendency, which will be discussed in section 2.3.1.

Besides the water quality parameters, the effect of liquid velocity on the corrosion rate is also important to take into account. According to several studies, the critical velocity above which the corrosion rate decreases, because of the supply of oxygen for the formation of a passive film, is about 0.7 m/s [35,36]. On the other hand, high water velocities can prevent the formation of passive films through the action of shear stress.

2.2.4 Corrosion inhibitors

Treatments against electrochemical corrosion involves eliminating at least one of the four requirements of the electrochemical cell, described in Section 2.2.1. *Corrosion inhibitors* are chemical substances that are used to reduce the corrosion rate. Corrosion inhibitors can have three common actions on an iron surface. First, the inhibitor can directly oxidize the ferrous ions to a stable ferric oxide near the metal surface. Second, the inhibitor can catalyze the reaction of oxygen with the ferrous ions. Third, the inhibitor can adsorb onto the surface to from a barrier or adsorb onto the oxide layer to strengthen the protective film.

Another way of categorizing corrosion inhibitors is by subdividing the inhibitors in three categories, namely anodic inhibitors, cathodic inhibitors, and film-forming inhibitors. *Anodic inhibitors* interfere with the anodic reaction and are applied to prevent dissolution of the metal and to prevent aggressive ions from reaching the metal surface. Although anodic inhibitors enhance the formation of a protective oxide layer, a minor defect in the oxide film creates small anodic sites that suffer from high corrosion rates, which results in pitting. *Cathodic inhibitors* interfere with the cathodic reaction and are applied to prevent electron transfer at the cathode and the reduction of oxygen. *Mixed inhibitors*, which are mostly organic inhibitors, provide a protection mechanism that relies on the adsorption of the inhibitors, this can be either physical adsorption, chemisorption or film formation. Chemisorption is more effective than physical adsorption because it is non-reversible in many cases [37]. Adsorption relies on the structure of the inhibitor, the surface charge of the metal, and on the type of electrolyte [38]. Just like in the case of anodic inhibitors, minor defects can result in high corrosion rates.

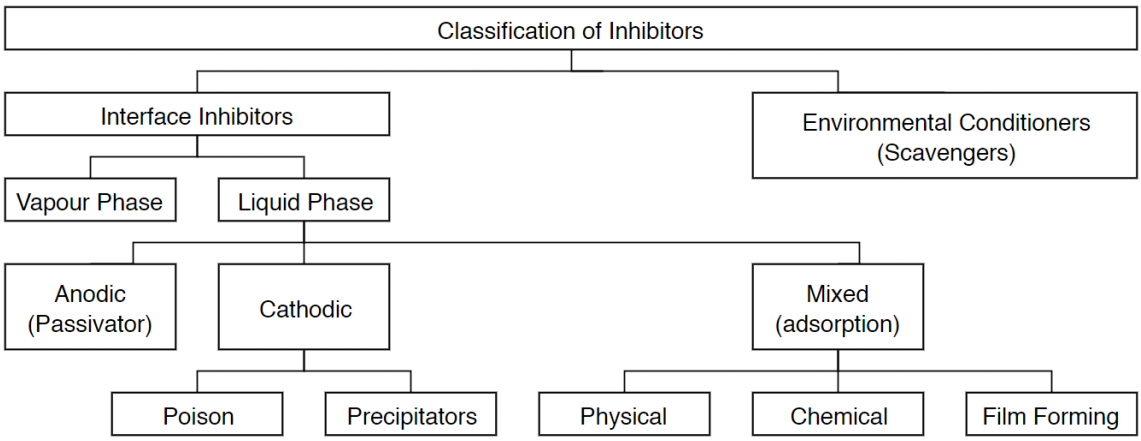

Figure 7: Classification of inhibitors (based on diagram in Uhlig's Corrosion Handbook [38])

Most corrosion inhibition programs rely on more than one type of inhibitor. A combination of different inhibitors can reduce the total dose required. Effective inhibitors for SACW could contain molybdate, zinc, amines or phosphonates. These inhibitors can be toxic at the required concentrations, while phosphorus and nitrate containing inhibitors stimulate undesired microbiological growth in the CWS and cause eutrophication of the environment. The debate on silica as corrosion inhibitor is mature but still ongoing, since the silica chemistry is complex and different for each type of water.

The selection of inhibitors for the corrosion experiments in this research was based on the criterion of non-toxicity for the environment and on the availability for the experiments. The first selected inhibitor was the organic film forming inhibitor created by Novochem Water Treatment called NovoTraqua® (NT), and the second inhibitor was $Na_2SiO_3 \cdot 5H_2O$ of Sigma Aldrich (≥95.0%). Additionally, a Conventional All Organics (CAO) inhibitor was used, as this type of inhibitor is common for alkaline environments.

Organic inhibitors often contain one or more of the heteroatoms, N, O, S, P, or Se, through which the inhibitors anchor to the metal surface [38]. These functional groups act as an adsorption center in the inhibitor molecule and adsorbs to the metal surface. NT is an organic inhibitor that relies on both physical adsorption and chemisorption. It protects the metal by blocking and by hydrophobic effects. The heteroatom of this inhibitor is O and the anchoring functional group is $-COO^-$. The polar heads of the surfactants orientate towards the metal surface, resulting in outward facing hydrophobic groups that repel the cooling water An important benefit of NT is its biodegradability and its non-toxicity. The standard NT product contains phosphonates at a concentration of 7.08% total-PO_4^{3-}.

All-organic treatment programs frequently incorporate phosphonates, which are very stable and can operate at high alkalinities [39,40]. Phosphonates can act as both anodic inhibitor, by catalyzing the oxidation of $Fe(OH)_2$, and as cathodic inhibitor, if calcium or magnesium is present,

to form a scale barrier film. So the efficiency of corrosion inhibitors containing phosphonates in SACW cannot rely on the cathodic inhibitor function.

Sodium silicate, or waterglass, is a corrosion inhibitor for soft waters that is appropriate in terms of non-toxicity, non-phosphate, cheap and available [41]. Silica provides protection to iron by forming an amorphous silica film which prevents the iron from dissolution. Lehrman and Shuldener [42] state that solid corrosion products of the metal must be present before silica is taken up from the solution. The negatively charged siliceous species react with the positively charged iron ions. Despite its application, the inhibitive effects and mechanisms of sodium silicate as corrosion inhibitor are not well understood and research is ongoing [40].

2.3 Corrosion measurements

2.3.1 Corrosion indices

No general corrosion index for predicting corrosion rates is available although several attempts have been made. The developed indices often apply to specific cases only or are based on the assumption that $CaCO_3$ scale formation, as a protective layer on the metal surface, is possible. In the case of soft water, where the Ca^{2+} and the Mg^{2+} ions are removed, the corrosion indices based on scale formation are not suitable. This is also true for one of the most common saturation indices, the Langelier index [8].

There are a number of water quality parameters that must be considered in the development of a corrosion index or a series of indices. These include: hardness, alkalinity, carbonate, carbon dioxide, pH, chloride, sulfate, ionic strength, conductivity, TDS, color, hydrogen sulfide, buffer capacity, phosphate, silicate, DO, chlorine (free or combined), and temperature [7]. The corrosion index must be designed so that the protective mechanism for a given water would predominate in the calculation of the index.

Two corrosion indices that may be used as a rough estimate for the corrosion susceptibility are the Larson-Skold index [9] and the Riddick index [10], which describe the corrosivity of water on empirical bases. The Larson-Skold index (LSkI) is established on an empirical relationship between polarization tests and mass loss determinations and is confirmed by Stern and Geary [43]. The study by Larson and Skold revealed a corrosivity relationship between the inhibiting property of bicarbonate and the chloride and sulfate concentration, given in Equation (2.13) where all concentrations are expressed as mg $CaCO_3$/L.

$$LSkI = \frac{\left[Cl^-\right] + \left[SO_4^{2-}\right]}{\left[HCO_3^-\right] + \left[CO_3^{2-}\right]} \tag{2.13}$$

The index can be interpreted by the guidelines given in Table 1.

Table 1: Interpretation guidelines for the LSkI

LSkI	Indication
< 0.8	chlorides and sulfate probably will not interfere with natural film formation
0.8 - 1.2	chlorides and sulfates may interfere with natural film formation and higher than desired corrosion rates might be anticipated
> 1.2	the tendency towards high corrosion rates of a local type should be expected as the index increases

The Riddick Index is also an empirically developed index but takes more factors into account that contribute to or that can mitigate the corrosion. The values obtained applied well to the soft waters of the eastern seaboard of the United States but not to harder waters of the middle part of the country [7]. The total hardness is defined by the calcium (Ca^{2+}) and the magnesium (Mg^{2+}) concentration as equivalent parts per million $CaCO_3$.

$$RI = \frac{75}{Alk}\left[CO_2 + \tfrac{1}{2}(Hardness - Alk) + Cl^- + 2N\right]\left(\frac{10}{SiO_2}\right)\left(\frac{DO+2}{Sat.DO}\right) \qquad (2.14)$$

Where

CO_2	Free CO_2 Concentration (mg/L)
Hardness	Hardness (mg/L as $CaCO_3$)
Alk	Alkalinity (mg/L as $CaCO_3$)
Cl^-	Concentration (mg/L)
SiO_2	Concentration (mg/L)
N	Concentration (mg/L)
DO	Dissolved oxygen (mg/L)
Sat.DO	Oxygen saturation at atmospheric pressure (mg/L)

Table 2: Interpretation guidelines for the RI

RI	Indication
0-25	non-corrosive
26-50	moderately corrosive
51-75	corrosive
>75	very corrosive

Pisigan and Singley [32] proposed to combine the composite effect of pH and alkalinity into one parameter, the buffer capacity β. The attempt was made to relate the buffer capacity to the corrosion rate, but no definable relationship was found.

2.3.2 Mass loss measurements

The average corrosion rate over a specific period of time can be calculated by measuring the mass loss of the specimen before and after immersing it in a corrosive environment and is calculated with Equation (2.15). The corrosion products need to be removed by etching before weighing. The duration of the tests depends on purpose of the test. Common testing periods for laboratory immersion corrosion testing of metals is 1 to 10 days. [44]

$$R = \frac{KW}{ATd} \tag{2.15}$$

Where:

K	= a constant for calculating the corrosion rate in the right units;
	= 3.45×10^6 for mpy
	= 8.76×10^4 for mm/y
W	= mass loss in g, to the nearest 1 mg (corrected for any loss during cleaning)
A	= area in cm^2 to the nearest 0.01 cm^2
T	= time of exposure in hours to the nearest 0.01 h;
d	= density in g/cm^3 which is 7.86 g/cm^3 for carbon steel.

Corrosion inhibitors are generally applied to decrease the corrosion rate. The efficiency of the corrosion inhibitors is calculated with Equation (2.16).

$$IE = \frac{w_0 - w}{w_0} \tag{2.16}$$

Where w_0 is the corrosion rate in the absence of inhibitor and w is the corrosion rate in the same environment in the presence of the corrosion inhibitor. The corrosion rates can be expressed in mils per year (mpy) or millimeter per year (mm/y) for example.

2.3.3 Voltammetry

Voltametry is a category of electroanalytical methods that can obtain information on the corrosion behavior of a metal sample by controlling the potential and measuring the resulting current density in a corrosion cell comprising of two or three electrodes. The potential of a system has to be measured to a certain reference, which requires a reference electrode (RE). One type of conventional reference electrode is the Saturated Calomel Electrode (SCE) that has a reference potential of +0.241 relative to the Standard Hydrogen Electrode (SHE). The corrosion potential of a system is determined by measuring the *open circuit potential* (OCP) that exists between the metal sample, which is the working electrode (WE), and the reference electrode. In *potentiodynamic polarization tests*, the potential is changed in a controlled manner using the WE and RE, while the resulting current density is monitored using the WE and an auxiliary electrode (AE). Common materials for auxiliary electrodes are graphite and platinum.

Current density versus potential plots are established by polarizing the WE by an external source, the *potentiostat*. The obtained anodic and cathodic polarization curves establish the *Tafel-plot* of which an example is given in Figure 8. The corrosion potential and current can be determined at the intersection of the linear derivative of the anodic and cathodic branch in the Tafel-plot because the corrosion rate depends on the equilibrium kinetics of the oxidation and reduction reactions. Faraday's law describes the linear relationship between the corrosion rate *R* (or metal dissolution rate) and the corrosion current i_{corr} as is given in (2.17).

$$R = \frac{M}{nF\rho} i_{corr} \tag{2.17}$$

Where *M* is the atomic weight of the metal, *n* is the charge number, *F* is the Faraday constant, and ρ is the metal density.

The resulting polarization curves show the corrosion behavior under cathodic or anodic polarization, and indicate the regions of immune, active, passive, transpassive behavior, as is shown in Figure 9.

Cyclic voltammetry is a *cyclic potentiodynamic polarization* (CPP) test in which the potential is reversed after reaching a potential or current density setpoint. CPP tests are performed to evaluate the susceptibility to pitting initiation and propagation. A large increase in the current density marks the initiation and propagation of localized corrosion, which is called the *breakdown point*. The potential is reversed after the local breakdown of the passivity. If the specimen is able to repassivate after the breakdown, the current density will also decrease again. If the specimen is not able to repassivate, the current density will remain high with decreasing potential. Increasing the potential without breakdown of the passivity, *oxygen evolution* as in Equation (2.8) can be observed. The possible CPP curves are described in Figure 10, where E_{ocp} is the OCP, E_b is the breakdown potential and E_p is the repassivation potential.

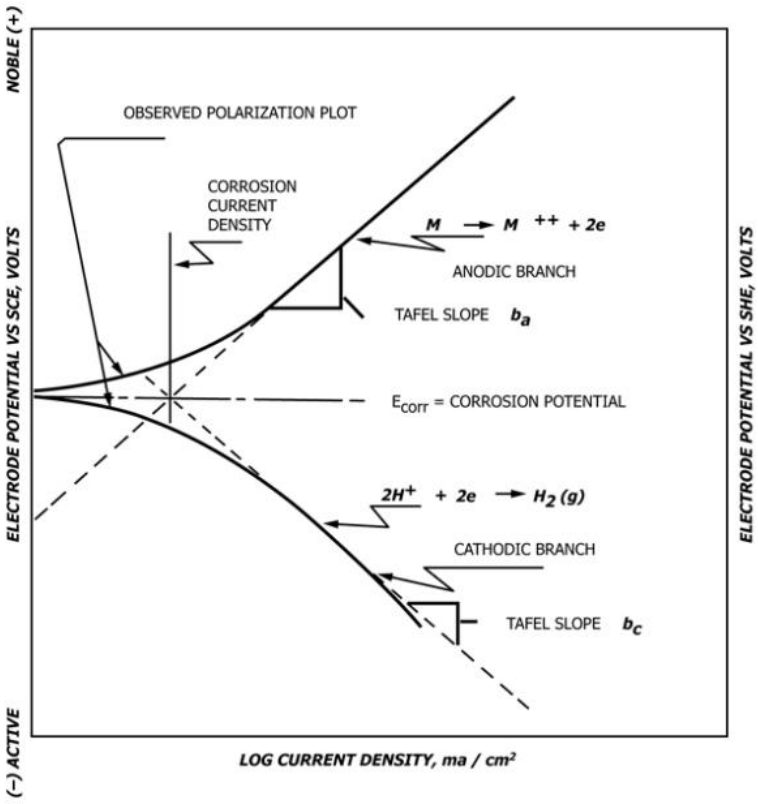

Figure 8: Hypothetical cathodic and anodic polarization diagram (ASTM G3 [45]).

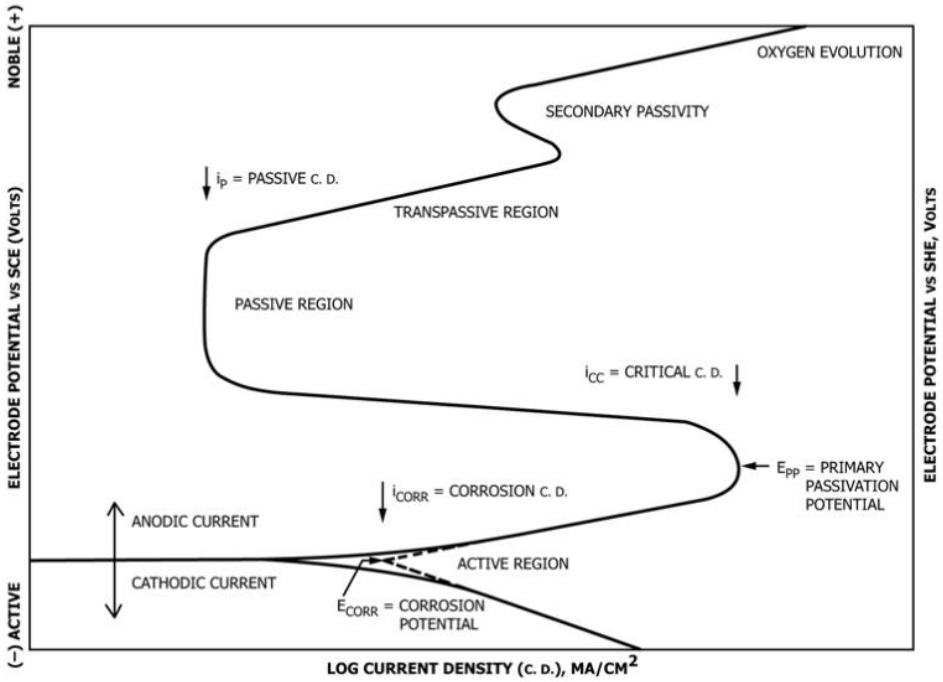

Figure 9: Hypothetical cathodic and anodic polarization plots for a passive anode (ASTM G3 [45]).

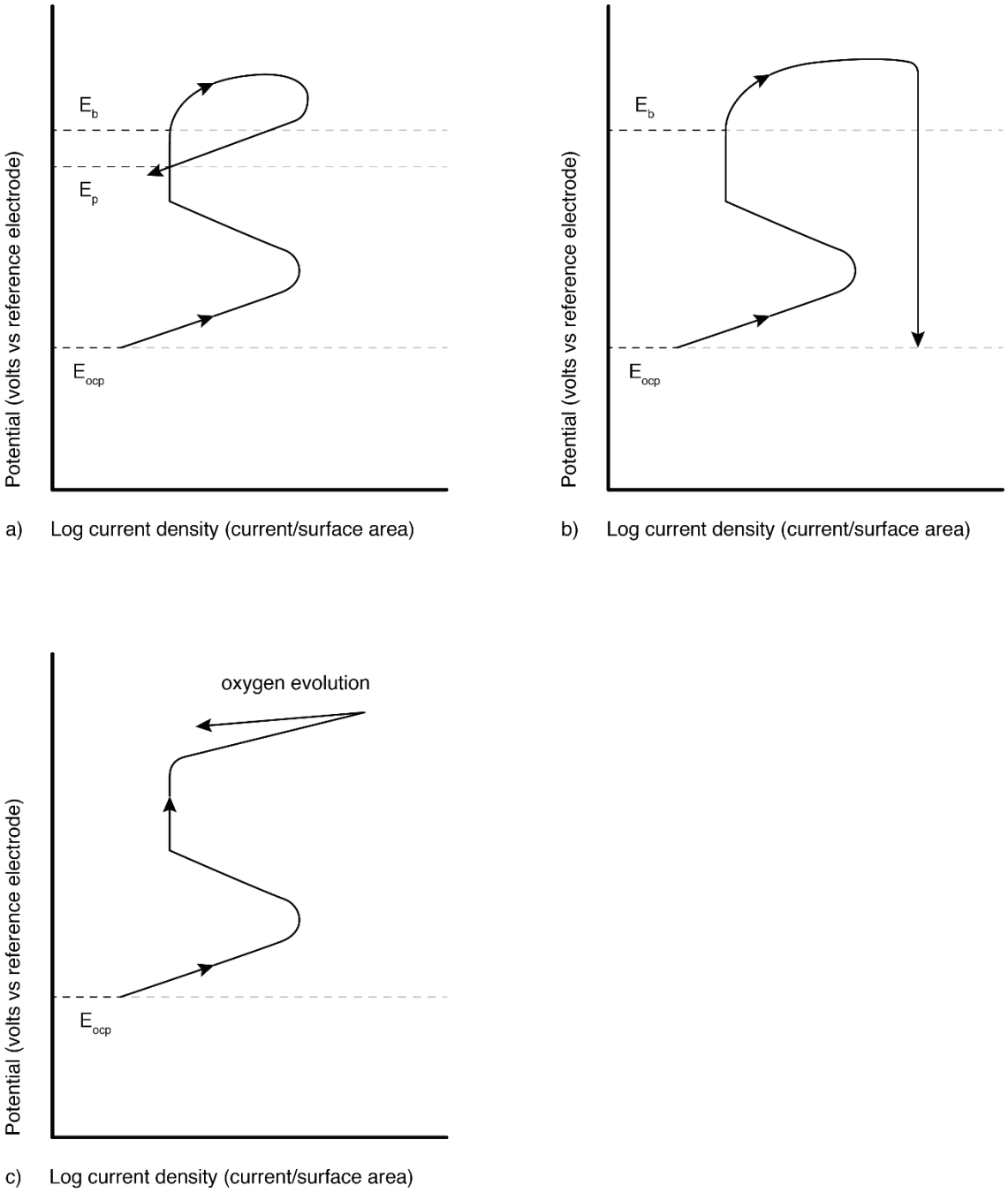

Figure 10: Hypothetical CPP diagrams where a) the sample is repassivated after local passivity breakdown, b) the sample is not repassivated after local passivity breakdown, and c) the breakdown point is not reached and oxygen evolution occurs.

2.3.4 Surface analysis

Different surface analyses techniques are useful for a better understanding of corrosion behavior and for verification of results obtained by mass loss tests and electroanalytical methods. Scanning electron microscopy (SEM) in combination with energy dispersive spectroscopy (EDS) is a common method in corrosion research used to study the surface morphology and to determine the composition of the top layer of the specimens on a microscale. SEM/EDS collects information of the sample its surface by scanning the surface with a focused beam of electrons in a vacuum chamber. The beam of electrons excites the atoms of the specimens surface resulting in a characteristic backscatter of electrons released by the specimen, which gets translated to an image or elemental analysis based on the energy that is transmitted by the electrons of the exited atoms. SEM could create images from nanosized areas because this surface analysis technique does not rely on the magnifying power of an objective lens. While SEM is used to create images, EDS is used for the elemental analysis of the surface of a sample. (E. Reinton, personal communication, March 1, 2018)

Another advanced surface analysis method is X-ray diffraction (XRD). This method can determine the crystalline structure of the top layer of a specimen. A beam of send X-rays gets diffracted by the top layer of the specimen and the angles and intensities of the reflected beams are used to identify the crystalline structure. Amorphous layers will not diffract the X-rays in an identifiable pattern. (R. Hendrix, personal communication, September 27, 2017)

3 Synthetic Cooling Water

The lab experiments that tested the corrosion behavior of mild steel in CWS were executed in water that resembled the main characteristics cooling water. Three different types of cooling water were considered for the experiments, actual cooling water from on-site, lab-concentrated surface water, and synthetic cooling water. The first option, actual cooling water, could have been obtained from a site in the Botlek operated by Evides Industrial Water. The second option, concentrated surface water, could have been obtained by applying small scale treatment steps to surface water, followed by a concentration step by means of a reverse osmosis (RO) membrane. The surface water was available from a pipeline that transported water to the laboratory from a nearby major water canal. The surface water would have been concentrated by recirculating the concentrate stream from the RO membrane to reach the desired concentration ratio. The third option, synthetic cooling water (SCW), comprised ultrapure water as a base matrix and a well-defined dosage of different salts.

The two key criteria for selecting the type of cooling water that would be used in lab experiments were repeatability and representability. An additional criterion was self-sufficiency. Out of the three options, SCW was selected based on these criteria. This chapter describes how the SCW was produced, what the characteristics were and how the calculations compared with the results calculated by the software PHREEQC with the proposed synthetic water composition as input file.

3.1 Materials and Methods

3.1.1 Synthetic cooling water production

The composition of the SCW was derived from the composition of Dutch surface water. Table 3 gives an overview of the main water constituents of three surface waters in the area that are indirectly used for cooling water. Based on the values of these three water bodies, values for synthetic surface water were selected. The COC determined with what ratio the ion concentrations of the SSW must increase to obtain SCW. Depending on what COC was selected the desired ion concentrations and therefore the required salt dosages could be calculated. The procedure for making SCW was based on the Dutch protocol for preparing synthetic laboratory samples [46], a guidance on metals in aqueous media [47], and a standard for the preparation of substitute ocean water [48].

Table 3: Main water composition of the river Meuse at Keizersveer (RIWA), the surface water reservoir Peterusplaat (Evides), the surface water reservoir Braakman (Evides) and the selected guideline for the SSW composition.

		Keizersveer	Petrusplaat	Braakman	SSW
pH	(-)	7.94	8.53	8.02	-
Temp	(°C)	13.2	12.4	13.2	-
EC	(µS/cm at 20°C)	472	419	572	564
TOC	(mg/L)	4.8	4.1	8	5.1
HCO_3^-	(mg/L)	169	126	194	145
Na^+	(mg/L)	31.5	32	38	32
K^+	(mg/L)	6.6	6.4	12	8
Ca^{2+}	(mg/L)	58.1	49	74	60
Mg^{2+}	(mg/L)	-	7.3	10	8
NH_4^+	(mg/L)	0.145	0.06	0.03	0.1
Cl^-	(mg/L)	44.8	45.5	66.4	46
SO_4^{2-}	(mg/L)	50.3	50	56	52
NO_3^-	(mg/L)	14.5	10.3	13.7	13
P-tot	(mg/L)	0.39	0.3	0.013	0.35
Fe-tot	(mg/L)	0.61	0.013	0.04	0.1
Mn	(mg/L)	0.674	0.01	0.01	0.01
F	(mg/L)	0.229	0.21	0.2	0.21
Br	(mg/L)	0.0935	0.08	-	0.09
SiO_2	(mg/L)	2.56	2.1	1.7	2.2

The total organic carbon (TOC) in the SCW was simulated by dosing humic substances. Commercial humic substances, like sodium humic acids of the brand Sigma Aldrich, are considered inappropriate for the simulation of surface water [49]. As an alternative, the product HumVi was used. This is a concentrated and desalinized product from the regenerate stream of the ion exchange process in the drinking water production line of Spannenburg, Vitens N.V. and is high in fulvic acids. Fulvic acids are the main form of humic substances in surface waters [50]. Additional information on HumVi is provided in Appendix A. Although the remaining salt concentration of HumVi is low, it is accounted for in the calculation of the required salt dosages of the SCW.

The different ions in the SCW can precipitate under certain conditions. Iron, manganese, calcium and magnesium precipitate at a high pH, whereas the solubility of silica in water increases above pH 8 [51]. In case SCW with a COC of 10 is prepared containing all components listed in Table 3, multiple stock solutions have to be prepared that favor the solubility of the different components. These stock solutions are at least a tenfold more concentrated than the SCW that is used in the experiments. This means that when a COC of 10 is used in the experiments, the stock solutions must be at least a COC of 100. These solutions are prepared with high purity chemicals and ultrapure water, as is summarized in Table 4.

Table 4: Chemicals used to create the stock solutions to produce SCW.

	Brand	**Purity**	**Molar mass**
	(-)	(%)	(g/mol)
Stock sol. A			
Na_2SO_4	Sigma Aldrich	≥ 99.0	142.04
NaCl	VWR	≥ 99	58.44
$NaNO_3$	Sigma Aldrich	≥ 99.0	85.00
KCl	Sigma Aldrich	99.0-100.5	74.55
Na_3PO4	Sigma Aldrich	96	163.94
NaF	Sigma Aldrich	≥ 99	41.99
NH_4HCO_3	Sigma Aldrich	≥ 99.5	79.06
NaBr	Sigma Aldrich	≥ 99.5	102.89
HumVi	Vitens	See App. A	-
Stock sol. B			
$Na_2SiO_3 \cdot 5H_2O$	Sigma Aldrich	≥ 95.0	212.14
NaOH	Sigma Aldrich	≥ 97.0	40.00
Stock sol. C			
$FeCl_3 \cdot 6H_2O$	Sigma Aldrich	≥ 98	270.30
$MnSO_4 \cdot H_2O$	Sigma Aldrich	99.0-101.0	169.02
$CuSO_4$	Sigma Aldrich	98	159.61
H_2SO_4	Sigma Aldrich	95.0-98.0	98.09

Three stock solutions were proposed:

- Stock A: Bulk solution with soluble salts;
- Stock B: Silicate solution with raised pH;
- Stock C: Transition metals solution with lowered pH.

The preparation of the stock solutions was done in volumetric flasks. The volumetric flasks were acid-cleaned and rinsed with demineralized water. The mass of the chemicals was determined on a mass balance with a minimum display of 0.01 mg. The chemicals were dissolved in the volumetric flasks that was filled for 90% with ultrapure water. The pH of the water for stock solution B and C was adjusted, with NaOH and H_2So_4 respectively, before the other chemicals were dosed. After the last dosage, the flask was filled up with ultrapure water to reach the 100% of the required volume. The solution was mechanically mixed by a magnetic stirring rod during the dosages of the chemicals and another 24 hours afterwards. The stock solution was stored in a glass bottle that was closed to the surrounding air, in the dark, at approximately 4°C until use, and during a maximum of two months.

The three stock solutions were diluted and mixed upon usage to the desired COC. The mixture was left to age for 24 hours under continuous mixing and was used for a maximum of 1.5 weeks in the experiments. The SCW mixture required aeration with air from the atmosphere to ensure that the concentration of dissolved oxygen reached 100% saturation and that a CO_2 equilibrium of an open CO_2-system was reached.

The stock solution and the mixture were analyzed for pH, electrical conductivity (EC) and concentration of the components. Ion chromatography was used to measure the concentration of Ca^{2+}, Mg^{2+}, Na^{+}, K^{+}, NH_4^{+}, F^{-}, Cl^{-}, Br^{-}, NO_2^{-}, NO_3^{-}, SO_4^{2-} and PO_4^{3-} by means of the 883 Basic IC Plus in combination with the 881 Compact IC pro of the manufacturer Metrohm. Total carbon and inorganic carbon measurements were used to determine the TOC by means of the TOC-V CPH in combination with the ASI-V of the manufacturer Shimadzu. The iron and copper concentrations were measured using Merck Millipore test kits and the silica concentration was measured using Hach Lange test kit.

The calculations of the EC were based the Nernst-Einstein equation that relates the molar limiting conductivity and the diffusion coefficient for a given ion. The method of Appelo [52], who adapted this equation, was used to calculated the EC. The EC-values of the water at different temperatures were corrected using linear Taylor expression obtained from the non-linear compensation model and the parameters of Atkins [53], resulting in the following more simple equation:

$$EC_{25} = \frac{EC_T}{(1 + 0.020(T - 25))} \tag{3.1}$$

The aqueous solution must be electrically neutral. Because the SCW was based on surface water composition reports of which the reported values may have an electrical imbalance, the resulting SCW may also have an electrical imbalance. The charge-balance error (CBE) is calculated according to Equation (3.2) and a CBE of 5% or less is acceptable [54].

$$CBE = \frac{\sum cations - \left|\sum anions\right|}{\sum cations + \left|\sum anions\right|} \times 100 \tag{3.2}$$

3.1.2 PHREEQC

The water in a CWS is in contact with the atmosphere and changes temperature when passing the heat exchanger or during the evaporation process. The water quality is therefore rather dynamic. The SCW used in the lab experiments to test corrosion was under constant conditions. The outcomes of the PHREEQC model helped to verify whether a sound composition was selected for the concentrated SCW, whether the calculations were correct and what kind of precipitation products were to be expected. The precipitation products are based on the equilibrium phases specified in the PHREEQC database.

The pH is initially provided in the input file but is corrected by the partial pressure of CO_2 for an open system. The CO_2 concentration of the water exiting the piping system and entering the free atmosphere of the cooling tower is 800 ppm [55]. The partial pressure used in the input file is therefore $10^{-3.1}$ atm. The evaporation or the increase in COC is simulated by removing stepwise moles of water from the solution. The PHREEQC input file can be found in Appendix B.

3.2 Results and Discussion

3.2.1 SCW composition

It was decided that the SCW would resemble cooling water with a COC of 10. Advanced makeup water treatment would only be economically viable if high COCs are possible. The high ion concentrations and the resulting high pH level of cooling water with a COC of 10 would make it interesting to research the corrosion behavior and seek for alternative treatment opportunities.

Some simplifications were made in the final composition of the SCW. In practice, strong cation exchange (CIEX) could be applied to remove the hardness. For the composition of the SCW, it was assumed that Ca^{2+} and Mg^{2+} were completely exchanged by Na^{+} although CIEX does not have a 100% exchange efficiency. The concentrations of Cu^{2+} and Mn^{2+} are very low and would normally decrease even more after CIEX. Therefore, these ions were removed from the water composition.

Another simplification was the removal of HumVi from the initial SCW composition. TOC can increase the solubility of compounds that would have precipitated without the presence of TOC. The corrosion behavior of mild steel is also influenced by humic acids without knowing exactly by what mechanism and under which conditions. Therefore it was decided that HumVi is not included in the production of SCW.

The last component that was removed from the original composition was Fe^{3+}. Fe^{3+} ions precipitate at the natural pH of the SCW. Electrochemical measurements would have been undesirably affected by the precipitation products.

These simplifications resulted in a far easier procedure to produce SCW. First of all, a bucket was filled with 20 L ultrapure water. Subsequently the different chemicals and their dosages, as summed up in Table 6, were put in a small container. At last the dry mix of chemicals was slowly added to the water while the water was continuously stirred.

The final composition of the SCW is presented in Table 5 and the dosages to make this composition is given in Table 6. The carbonate equilibrium was selected at pH 9.5 and at 20°C, which resulted in 0.1% H_2CO_3, 88.3% HCO_3^- and 11.6% CO_3^{2-} based on the equilibrium equations of Harned and coauthors [56,57]. The CBE for this composition is -0.36% which is a good equilibrium of the charges.

Table 5: SCW composition with a COC of 10.

pH	(-)	9.1 → 9.4
Temp	(°C)	20
EC	(mS/cm)	4.4 → 4.5
TOC	(mg/L)	0
HCO_3^-	(mg/L)	1251
Na^+	(mg/L)	1166
K^+	(mg/L)	80
Ca^{2+}	(mg/L)	0
Mg^{2+}	(mg/L)	0
NH_4^+	(mg/L)	1.0
Cl^-	(mg/L)	460
SO_4^{2-}	(mg/L)	520
NO_3^-	(mg/L)	130
P-tot	(mg/L)	3.5
Fe-tot	(mg/L)	0
Mn^{2+}	(mg/L)	0
F^-	(mg/L)	2.0
Br^-	(mg/L)	0.9
SiO_2	(mg/L)	20

Table 6: Dosages for SCW with a COC of 10.

	Dosage
	(mg/L)
Na_2SO_4	769
NaCl	639
$NaNO_3$	178
KCl	153
$Na_2SiO_3 \cdot 5H_2O$	73
Na3PO4	6.0
$FeCl_3 \cdot 6H_2O$	0
NaF	4.4
NH_4HCO_3	4.4
NaBr	1.2
$NaHCO_3$	1722 →1601
Na_2CO_3	292 → 366

3.2.2 PHREEQC

Actual mixtures, according to the dosages of Table 6, resulted in a pH of 9.1 and an EC of 4.4 mS/cm. These values were in line with the results from PHREEQC. The input values for the solution and the eventual solution according to this model are given in Figure 11. Since the desired pH for the corrosion experiments was 9.4, the $NaHCO_3$ and the Na_2CO_3 dosages were adjusted to 1601 mg/L and 366 mg/L respectively.

Simulating the effect of higher COCs on the saturation indexes and the pH in PHREEQC resulted in the graphs of Figure 12. The model gives an initial idea of possible scale formation that were to be expected in experiments with the SCW. Ca^{2+} and Mg^{2+} obviously cause large scaling problems. Softening the water would reduce the risk of scaling. However, silica can cause a persistent scale in both hard and soft water and it can form complexes with iron. Quartz and other crystalline silica polymorphs exhibit slow precipitation kinetics, while amorphous silica or silicates tend to precipitate rapidly as scale deposits via condensation polymerization [58]. An elevated pH can increase the solubility and diminish the risk of scaling. Silica and silicates can also be considered as corrosion inhibitors. This is a short and incomplete summation of the effects of silica and silicates. Further research on the risks and benefits of silica in SACW is required, especially on the precipitation of metal-rich amorphous silica and at elevated temperatures.

```
SOLUTION        1
units           mg/l
pH              9.4     CO2(g) -3.1
temp            20
Alkalinity      1588    as HCO3

Na      1166
K       80
Ca      0
Mg      0
Amm     1
Fe(+3)  0
Mn      0
Cu(+2)  0

S(6)    520     # SO4-2
N(+5)   130     #NO3-
P       3.5     as PO4
Cl      460
F       2
Br      .9
Si      20      as SiO2
END
```

```
                                                  pH  =   9.112
                                                  pe  =   4.000
                        Specific Conductance (µS/cm,  20°C)  = 4396
                                        Density (g/cm³)  =   1.00119
                                            Volume (L)   =   1.00263
                                   Activity of water     =   0.998
                                Ionic strength (mol/kgw) =   5.798e-02
                                   Mass of water (kg)    =   1.000e+00
                                Total carbon (mol/kg)    =   2.339e-02
                                Total CO2 (mol/kg)       =   2.339e-02
                                    Temperature (°C)     =  20.00
                                Electrical balance (eq)  =   7.469e-04
                    Percent error, 100*(Cat-|An|)/(Cat+|An|)  =   0.73
                                        Iterations       =   4
                                            Total H      = 1.110345e+02
                                            Total O      = 5.560590e+01
```

Figure 11: PHREEQC input solution (left) and output characteristics (right).

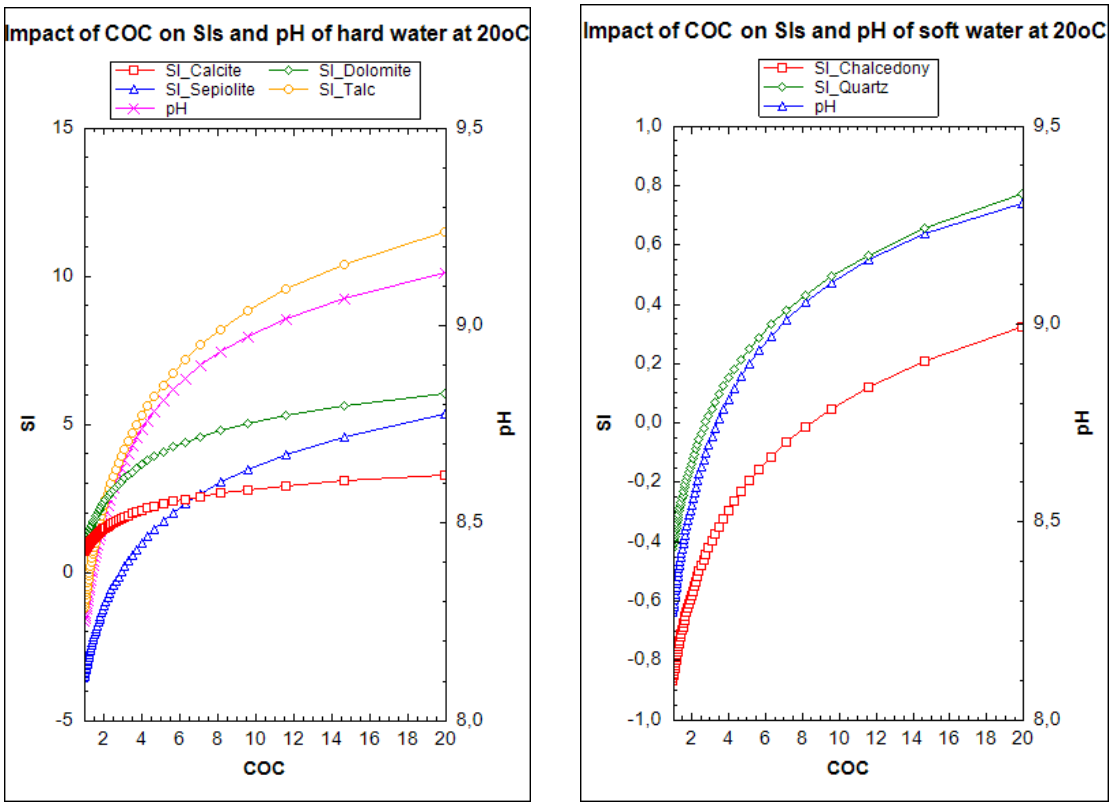

Figure 12: Impact of an increasing COC of SCW on the Saturation Index (SI) and the pH

3.2.3 Corrosion indices

The LSkI and the RI were calculated for the surface waters mentioned in Table 3, for the SSW and for the SCW. All waters were classified as moderately corrosive according to the LSkI and the COC of the water did not influence the value as was expected from evaluating the equation. An increase in the COC must however lead to an increase in the corrosion susceptibility as is experienced in practice.

The values according to the RI showed great variation that could be linked to the hardness concentration and alkalinity. The weight of *'hardness – alkalinity'* in equation is too large for the surface waters containing some hardness, even with the applied factor of $\frac{75}{Alk}\times\frac{1}{2}$. Singley [7] already stated that the index is not suitable for hard waters. In addition to this, it can be concluded that the RI is neither suitable for corrosion estimations of mild steel in Dutch surface waters. The RI for the SSW was classified as moderately corrosive while the RI for SCW was classified as non-corrosive. In this case mainly due to the high alkalinity of SCW.

The $\frac{DO+2}{Sat.DO}$ element in the index is not suitable for CWS since the water is oxygen saturated in these systems and oversaturated when heated at the heat exchangers. The absence of oxygen is beneficial for corrosion reduction, yet it should not be considered in this manner. The aim of SACW is natural passivation which requires oxygen. Therefore oxygen should have a beneficial effect on the corrosion reduction, and only if the water is oxygen saturated. Another element that is missing in the RI is the effect of SO_4^{2-}.

Although the limited application of corrosion indices was already stressed, it can be concluded that the corrosion indices that appeared to be most suitable for SACW of all corrosion indices, are unsuitable for corrosion estimations in this type of water.

4 Mass loss tests

Laboratory immersion corrosion tests were carried out to gain fundamental knowledge on the corrosion of mild steel in the SCW and the effect of different inhibitors on this corrosion process. Mass loss tests are the most common of all corrosion-test measurements for determining corrosion rates [59] and are widely applied in the field. Combining polarization resistance tests with mass loss tests can give useful insights. Mass loss measurements provide information on the average corrosion rate during a certain period, while polarization resistance tests provide information on the change in the corrosion rate during this period. This chapter will focus on mass loss tests and the subsequent surface analyses.

Two types of mass loss tests were defined in which the mass loss of metal coupons were determined; 48 hours immersion and 4 weeks immersion. The 48 hours tests were to provide an initial understanding on the corrosion behavior and are an uncomplicated method to generate an overview on the inhibition efficiency of different inhibitors, concentrations and conditions. Mass loss test should however run over longer periods of time to understand the development of the corrosion rate. Therefore a 4 weeks immersion test was designed that would provide information on the average corrosion rate per week during a period of four weeks.

This chapter describes first the coupon composition and coupon preparation, followed by a description of the setup, the test solutions, the surface analysis method and at last an overview of the procedures. The referenced standards that have been used as guidelines for creating an laboratory immersion test setup were:

- G1 Standard Practice for Preparing, Cleaning, and Evaluating Corrosion Test Specimens [60];
- G3 Conventions Applicable to Electrochemical Measurements in Corrosion Testing [45];
- G5 Standard Reference Test Method for Making Potentiodynamic Anodic Polarization Measurements [61];
- TM0169/G31 Standard guide for laboratory immersion corrosion testing of metals [44].

4.1 Materials and Methods

4.1.1 Coupon preparation and composition

The 48 hours immersion tests involved coupons that were made from cold rolled steel with the following composition (wt.%): 0.087 C, 0.375 Mn, 0.013 P, 0.013 S, 0.018 Si, and remainder Fe. The specimens had the dimensions of $80 \times 10 \times 1.5$ mm. The steel surface was prepared by mechanical wet grinding and polishing with silicon carbide paper of 320 to 1200-grit. Subsequently, the coupons were ultrasonically degreased with acetone for 15 minutes, rinsed with ethanol, rinsed with distilled water and dried in air. The mass of all the coupons was determined

on an analytical balance to the nearest 0.1 mg before the coupons were partially isolated from the environment with 3M™ polyester tape 8402 with silicone adhesive, leaving three circular areas of in total an area of 2.36 cm^2 to react with the environment. The adhesive has a high chemical resistance, also in anodizing environments [62], and is therefore suitable for the immersion tests. The specimens were finally stored in a desiccator and used for an experiment within one hour after storage.

The 4 weeks immersion tests involved standardized flat coupons with stamped identification numbers from Metal Samples Co with the chemical composition (wt.%): 0.08 C, 0.330 Mn, 0.011 P, 0.009 S, 0.045 Al, 0.019 Si, and remainder Fe. The dimensions of the coupons were 72 × 94 × 1.3 mm. The coupons were cleaned according to the same procedure as described for the 48 hours tests. No polishing was required (Novochem and Nalco, personal communication, 2017). For the 4 weeks immersion tests, the top 26 mm of the coupons, including the stamp, were isolated with the polyester tape, leaving an area of 46 × 9.4 × 1.3 mm to react with the environment. The dimensions of the exposed areas were determined with an accuracy of at least ±1% by using a digital Vernier caliper. Underneath the polyester tape, copper tape was applied to ensure a conducting connection between the sample and the potentiostat for polarization tests.

After the required immersion time and corrosion product analyses, the coupons were etched in an inhibited 3% HCl solution. The etching removed the corrosion product to unveil the metal surface and to determine the actual mass loss, again on an analytical balance to the nearest 0.1 mg.

4.1.2 Setup

The 48 hours tests implied a simple setup of acrylic containers with 210 mL of solution that was continuously stirred during 48 hours with a magnetic stirring bar. The metal surface of the coupon coupon was immersed in the solution in such a way that the rim of the polyester tape hung 1 cm under the water surface.

The setup for the 4 weeks immersion test consisted of six 2L polypropylene measuring jug in which four coupons could be immersed. A schematization and a photo of the setup are given in Figure 13 and Figure 14, respectively. The jugs were filled with a 1600 mL solution that was continuously refreshed with SCW that was pumped from a 10L bucket into the jug by a 205S Watson Marlow peristaltic pump. The pump had a capacity of twelve channels, of which six were assigned for the influent flow and six were assigned for the effluent flow. The effluent was pumped from the jugs into separate 2L polypropylene bottles. The hydraulic retention time was four days. The influent was air saturated at 1 atm by aerating the influent SCW with an aeration stone and stirring the water with a magnetic stir bar. All jugs were stirred with by the JLT6 jar test of Velp Scientifica by means of a mechanical mixer that created an average velocity of 1 m/s at the outer edges of the jugs. The minimum ratio of test solution volume to test specimen surface area of 0.20 mL/mm^2 was recommended by ASTM G31 [44]. With a total surface area of almost 1000 mm^2 for the four coupons and a solution volume of 1600 mL, this recommendation was met.

The measuring jugs were closed off with custom made lids, which included coupon holders, openings to mount sensors, and an opening for the mechanical stirring rod. The spout was closed off with plastic paraffin film. All material, other than the coupons, was made of plastic if possible. This was to avoid glass contamination. The lids were designed in such a way that they would also fit on the original glass beakers belonging to the JLT6 jar test. A photo of the jug and lid are given in Figure 15 and Figure 16. The coupons were mounted to the coupon holders with a plastic screw and nut, 3 cm above the water surface to avoid crevice corrosion. The length of the coupon holders ensured that the coupons were covered with polyester tape at the height of the water-atmosphere interface, to avoid water line corrosion. The coupon holders were located on the outer edges of the lid while the sensors were located in the center of the lid.

The sensors measured the pH, EC and the temperature every hour. The water temperature was manually regulated with a six position heating plate. Initial tests indicated that the temperatures were not sufficiently constant since they could vary ± 4°C among eachother. Therefore, the final tests were run at a room temperature of 21.0 °C ± 1.5°C and the heating plates were no longer used.

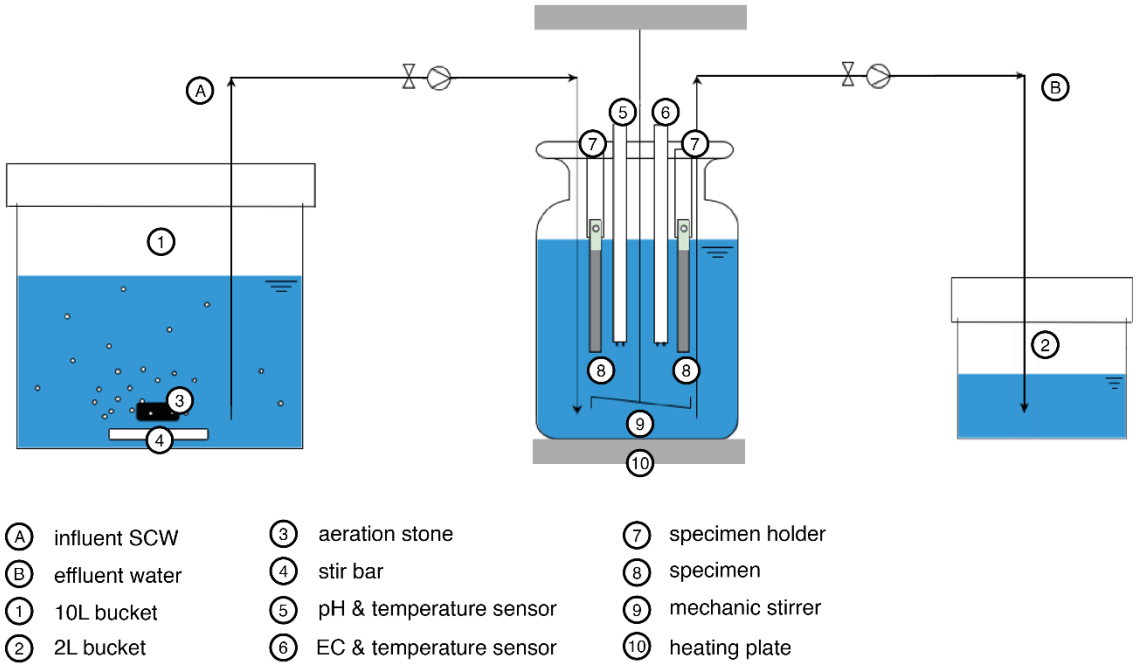

Figure 13: Schematic representation of the 4 weeks immersion test setup of a single jug.
(See Appendix C for the multiple jug setup schematization.)

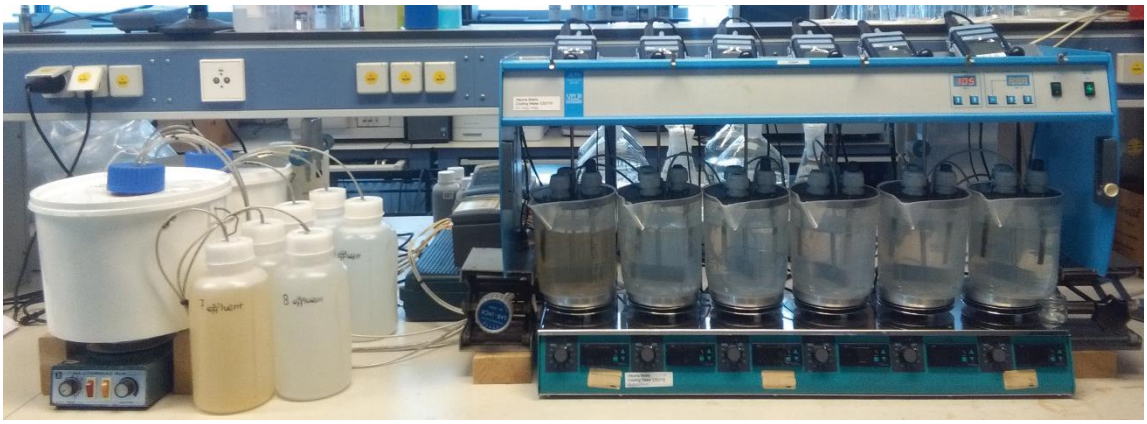

Figure 14: Photo of the 4 weeks immersion test setup.

Figure 15: 2L Measuring jug with custom made lid.

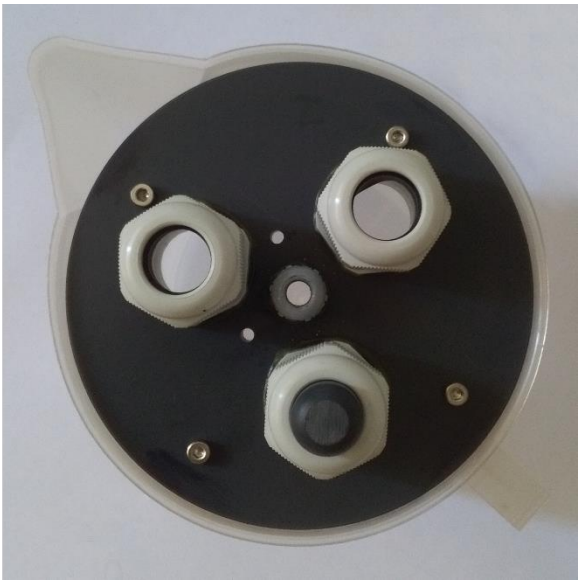

Figure 16: Custom made lid with fixed positions for coupon holders, sensors, stirring rod and influent and effluent syringes.

4.1.3 Test conditions

The experiments of the 48 hours immersion were started with four different solutions. Depending on the results, more solutions would be tested and all tests would be executed in triplicates. The four solutions that were tested in duplicates at first were:

- Blanc: only SCW;
- CAO: SCW with 200 ppm Conventional All Organics inhibitor;
- NT100: SCW with 200 ppm NT containing 100% of the original phosphorus concentration;
- Si200: SCW with 200 ppm SiO_2 dosed as $Na_2SiO_3 \cdot 5H_2O$.

These tests would have been followed up by immersion test with the following composition:

- NT50: SCW with 200 ppm NT containing 50% of the original phosphorus concentration;
- NT25: SCW with 200 ppm NT containing 25% of the original phosphorus concentration;
- NT12: SCW with 200 ppm NT containing 12.5% of the original phosphorus concentration;
- NT0: SCW with 200 ppm NT containing 0% of the original phosphorus concentration;
- Si300: SCW with 300 ppm SiO_2 dosed as $Na_2SiO_3 \cdot 5H_2O$;
- Si100: SCW with 100 ppm SiO_2 dosed as $Na_2SiO_3 \cdot 5H_2O$.

The solutions of the 48 hours experiments where not refreshed during those 48 hours. This was different for the solutions in the jugs of the 4 weeks immersion tests. Those solutions were continuously refreshed based on a hydraulic retention time of four days. The setup provided the possibility of running experiments in six jars simultaneously. Therefore, four different solutions were tested in triplicates during two months, namely Blanc, CAO, NT100 and Si200. The dosages of the inhibitors were calculated based on the HTI. The HTI of the setup, with a volume of 1600 mL and a hydraulic retention time of four days, was 2.8 days. Figure 17 shows the development of the inhibitor concentration over time if the inhibitor concentration decreases only due to SCW inflow and inhibitor outflow with the effluent. The inhibitors were dosed directly in the jugs with a Thermo Scientific Finnpipette. The inhibitors were dosed with a 24 hour interval, therefor the dosages were based on the desired concentration after 24 hours. This means that the required dosage for a system with a volume of 1600 mL and a desired concentration of 200 ppm, was 528 µL . A double inhibitor dosage was applied upon startup, as is common in practice to ensure full protection by the inhibitor.

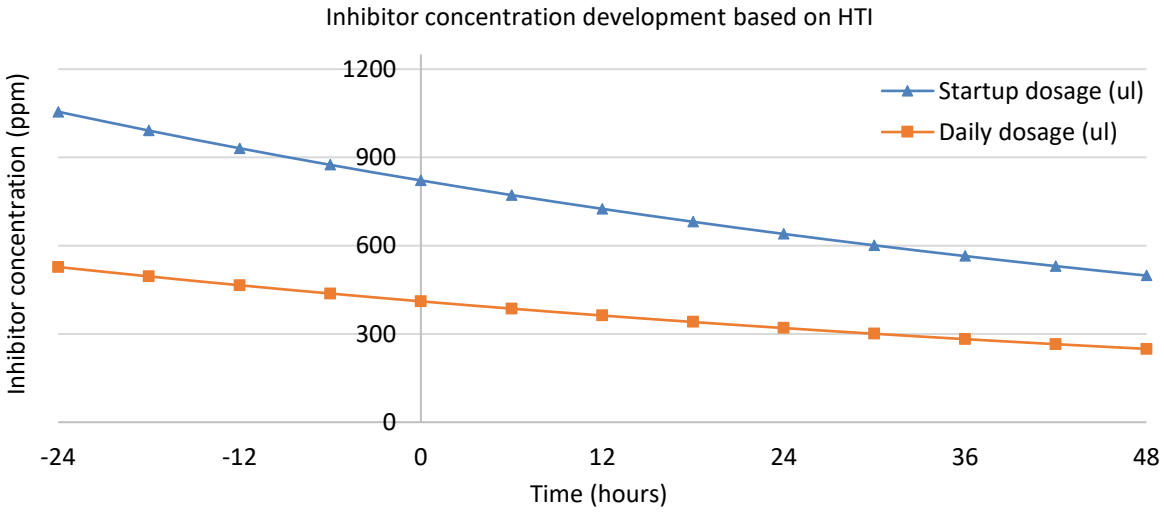

Figure 17: Inhibitor concentration development due to inflow of SCW and outflow of inhibitor with the effluent.

4.1.4 Surface analyses

The surfaces of the coupons were photographed and evaluated before immersion, after immersion when the corrosion products were still visible, and removal of the corrosion products by etching, which revealed the surface attack. The surface attack was categorized in uniform corrosion, crevice corrosion and pitting corrosion based on visual inspection with 15x magnification when necessary. The pitted surfaces were rated in terms of pit density based on the ratings in Table 7. Differentiation was made between the outward facing surface and the inward facing surface. Vertical cross-sectioning was required to determine the pit type as presented by Figure 6 [30], however this was not part of the scope.

Table 7: Rating table for pit density.

	Pit density (number of pits/m^2)
P-1	$<4 \times 10^3$
P-2	$<2 \times 10^4$
P-3	$<8 \times 10^4$
P-4	$<2 \times 10^5$
P-5	$>2 \times 10^5$

4.1.5 Procedure

The previous sections provide information on the coupon preparation, the setup, the test conditions and the surface analyses. This section provides a stepwise overview of the actions for the mass loss tests. The 48 hours immersion test was a simple test and its procedure is summed up below.

1. Coupon preparation as in Section 4.1.1;
2. Solution preparation as in Section 4.1.3;
3. The pH, EC and temperature of the solution were measured;
4. The coupon was immersed in the solution;
5. The coupon was removed from the solution after 48 hours;
6. The surface was photographed;
7. The tape was removed;
8. The surface was etched;
9. The mass of the coupon was determined;
10. The surface was photographed again;
11. Surface analyses was performed;
12. The coupons were numbered stored in small sealed bags.

The goal of the 4 weeks immersion test was to determine the average corrosion rate per week during a period of four weeks based on mass loss, and to determine the corrosion rate after two and four weeks. The results of the mass loss test and the polarization resistance tests were to be compared. The procedure of the 4 weeks immersion test is summarized on the next page.

At the startup of the 4 weeks immersion test:

1. Setup preparation as in Section 4.1.2;
2. Coupon preparation as in Section 4.1.1;
3. Solution preparation as in Section 4.1.3;
4. The pH, EC and temperature of the solution were measured;
5. SCW was pumped through the entire setup;
6. 4 coupons per jug were mounted to the lid and immersed in the solution;

During the 4 weeks:

7. The pH, EC and temperature of the solution were measured ervery hour automatically and manually every day;
8. One inhibitor dosage was applied every day around 3 PM;
9. One coupon per jug was replaced after 1 week and after 2 weeks of immersion;
10. The procedures 6 untill 12 of the 48 hour immersion test were followed for the removed coupons;
11. All coupons were removed after running the setup for 4 weeks;
    a) The coupons that were immersed for 2 and 4 weeks were eached moved to a separate container with effluent from the correstponding jug and connected to the potentiostat to run a polarization resistance test;
    b) The coupons that were immersed for 3 and 4 weeks followed the procedures 6 untill 12 of the 48 hour immersion test;

At the end of the 4 weeks immersion test:

12. The setup is cleaned with acid and rinsed with distilled water.

All mass loss measurements were done in triplicates. Blanc, CAO and NT100 were tested during the first run of four weeks with two jugs per solution. Si200, Blanc, CAO and NT100 were tested during the second run. For this run, three jugs were assigned to the Si200 solution and the remaining three jugs were assigned to the Blanc, CAO and NT100 solutions.

4.2 Results and Discussion

4.2.1 Mass loss measurements

The mass loss of mild steel coupons was studied in different solutions and in different set ups. No visual corrosion of the coupons was observed in the 48 hours immersion tests. This can be related to the protection of the mild steel by passivation, as will be further discussed in Chapter 5. The 4 weeks immersion tests did result in corrosion rates and inhibitor efficiencies, and will have the main focus in this section.

The mass loss of mild steel coupons was determined every week during a period of four weeks. Based on the mass loss measurements, the corrosion rates were calculated with Equation (2.15).

The resulting corrosion rates of the coupons in the different solutions are summarized in Figure 18. The error bars indicate a two-sigma confidence interval. A maximum corrosion rate of 2 mils per year (mpy) is an acceptable corrosion rate of mild steel in full scale CWS. However, this is not a justifiable maximum corrosion rate for laboratory immersion tests. The corrosivity of the solutions to mild steel should be determined in relative, rather than absolute, terms [63].

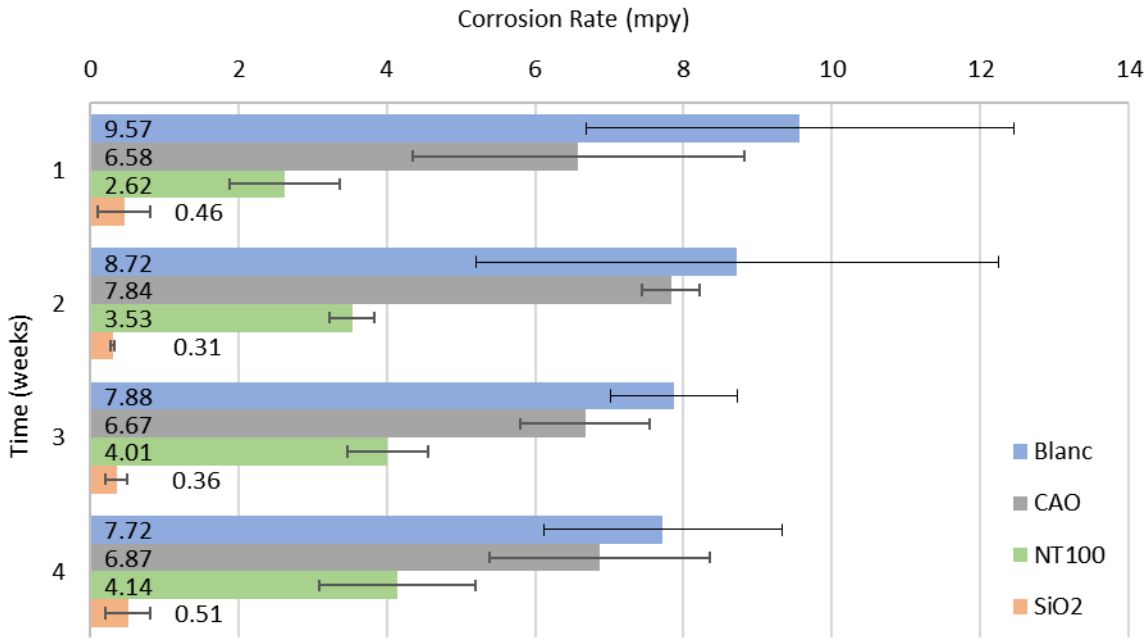

Figure 18: Corrosion rates for Blanc, CAO, NT100 and Si200 at a weekly interval.

The solution without inhibitors, i.e. Blanc, had the highest corrosion rates, followed by CAO, NT100 and Si200. This was conform the expectations because the addition of an inhibitor is supposed to lower the corrosion rates. Additionally, CAO is not designed for soft water and therefore provided only little protection against corrosion. The performance of NT100 was unknown so far for soft water at a pH above 9.3. The result was that it cut the corrosion rate of the Blanc solution by half. The inhibition efficiency of NT100 might have been higher if the concentration of inhibitor was increased. With this knowledge, the voltamettric tests described in the next chapter were carried out with higher concentrations. Si200 performed best of all inhibitors and no silica scale was observed in the system. Si200 is therefore considered as an inhibitor that is worthwhile to be further researched in soft alkaline cooling water conditions. The uncertainty was too large to state that the corrosion rates of one of the solutions decreased or increased during the four weeks period.

The inhibition efficiencies of CAO, NT100 and Si200 with respect to Blanc could be calculated based on the corrosion rates with Equation (2.16). Again, the effect of the uncertainty of the corrosion rates on the inhibition efficiency is too large to draw conclusions in terms of inhibition efficiency.

4.2.2 Surface analyses

Visual surface analyses were carried out to study the characteristics of the corrosion products before etching and of the surface of the coupon after etching. The analysis focused on uniform, crevice and pitting corrosion. It is possible that all three types of corrosion are found on a coupon. A distinction was made between the outward facing side of the coupon (F) and the inward facing side (B). Figure 19.a provides an overview of the number of coupons that exhibited uniform corrosion and Figure 19.b of the number of coupons that exhibited crevice corrosion, respectively. Figure 19.c provides an overview of the rating of the pit density based on the cut off values of Table 7. Where P-5 is an indication for a high pit density and P-0 for a low pit density, respectively. For each of the four solutions, twelve coupons were studied.

Although the uncertainty of the calculated corrosion rates was too large to state that the corrosion rate of the coupons in the Blanc solution decreased, the tendency may be true and be explained by the formation of a uniform protective layer of oxidation products. Mainly uniform corrosion and little pitting corrosion was identified on the coupons of the Blanc solution. With the formation of a uniform corrosion product on the steel surface, it is expected that the corrosion rate stabilizes over time.

It is important to note that most mass loss results were biased by crevice corrosion. The coupons in the Si200 solution suffered least from crevice corrosion, and also least from pitting corrosion. Particularly the coupons in the CAO and NT100 solutions suffered from pitting corrosion and partially or no uniform corrosion. Additionally, more uniform corrosion was observed on the inward facing side of the coupons which is related to a difference in the flow along the metal surface. Inserting coupons in a recirculating plug flow, like a corrosion rack, would diminish the effect of different flows along the coupon surface. So the bias of crevice corrosion, the non-corresponding types of corrosion among the coupons of the different solutions, and the difference between the inward and outward facing sides, made it faulty to draw conclusions in terms of best protection. It was right to conclude that calculating the inhibition efficiencies would be misleading. Still, it can be concluded that the Si200 solution has the best inhibiting effect on mild steel corrosion and further research on Si200 for this type of cooling water is recommended.

Electroanalytical methods in combination with surface examination were likely to provide more insights on the performance of the corrosion inhibitors and enable comparison between the different inhibitors. Since pitting was the main corrosion process in the solutions with an inhibitor, CPP tests were selected to evaluate the performance of the inhibitors. CPP tests are discussed in the next chapter.

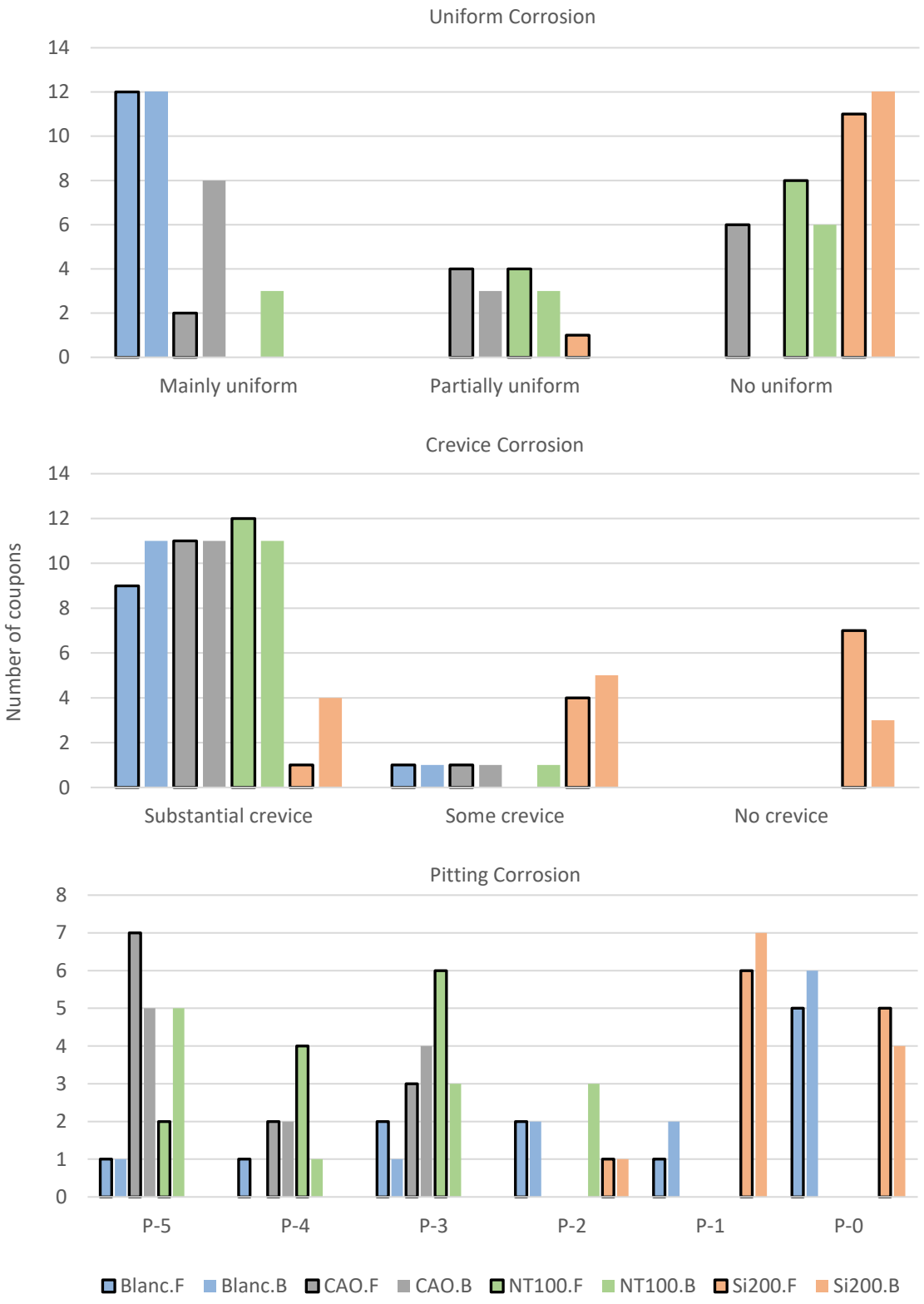

Figure 19: Results of surface analysis after immersion in terms of a) Uniform corrosion, b) Crevice corrosion, and c) Pitting corrosion. Distinction was made between the front/outward facing side of the coupon (F) and the back/inward facing side of the coupon (B).

5 Voltamettric tests

The behavior of mild steel in SCW in combination with different inhibitors and concentrations has been studied by means of cyclic potentiodynamic anodic polarization measurements (CPP) based on ASTM G61 [64]. This method provided an indication of the susceptibility to initiation of localized corrosion. The more noble the potential at which the anodic current increases rapidly, the less susceptible the alloy is to initiation of localized corrosion. The potential at which the hysteresis loop is completed is another indication of the likeliness of localized corrosion to occur. This chapter describes the experimental conditions and the results of the voltamettric tests in SCW. The standards that have been used for the voltamettric test as reference material are:

- F746 Standard Test Method for Pitting or Crevice Corrosion of Metallic Surgical Implant Materials [65];
- F2129 Standard Test Method for Conducting Cyclic Potentiodynamic Polarization Measurements to Determine the Corrosion Susceptibility of Small Implant Devices [66];
- G1 Standard Practice for Preparing, Cleaning, and Evaluating Corrosion Test Specimens [60];
- G3 Conventions Applicable to Electrochemical Measurements in Corrosion Testing [45];
- G5 Standard Reference Test Method for Making Potentiodynamic Anodic Polarization Measurements [61];
- G46 Standard Guide for Examination and Evaluation of Pitting Corrosion [30];
- G61 Standard Test Method for Conducting Cyclic Potentiodynamic Polarization Measurements for Localized Corrosion Susceptibility of Iron-, Nickel-, or Cobalt-Based Alloys [64].

5.1 Materials and Methods

5.1.1 Coupon preparation and composition

The experiments were carried out with specimens made from cold rolled steel with the following composition (wt.%): 0.087 C, 0.375 Mn, 0.013 P, 0.013 S, 0.018 Si, and remainder Fe. The specimens had the dimensions of $22 \times 22 \times 1.5$ mm. The steel surface was prepared by mechanical wet grinded and polished with silicon carbide paper of 320 to 1200-grit and ultrasonically degreased with acetone for 15 minutes, rinsed with ethanol, rinsed with distilled water and dried with pressurized air. The specimen was partially isolated from the environment with 3M™ polyester tape 8402 with silicone adhesive, leaving a circular area of 2.01 cm^2 to react with the environment. The specimens were finally stored in a desiccator and used in for an experiment within one hour after storage.

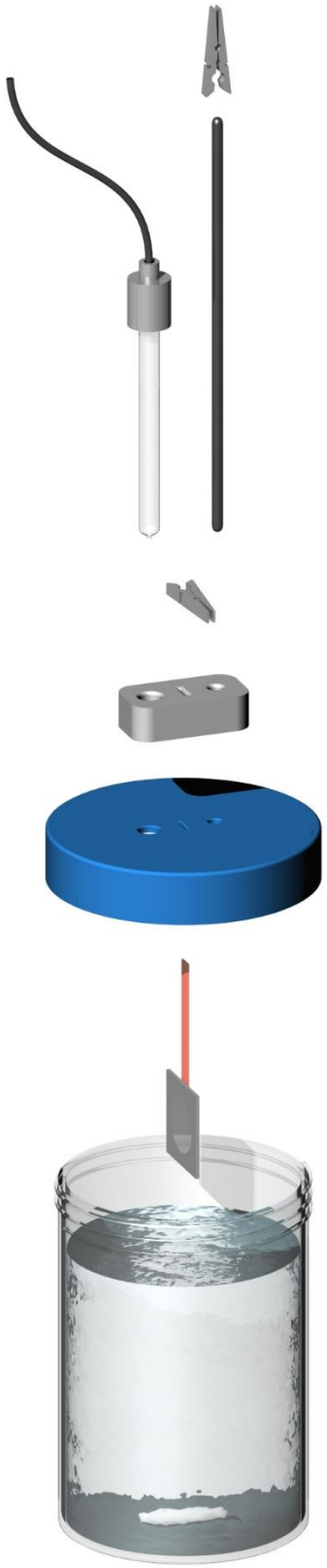

Figure 20: Corrosion cell set-up, exploded view with water.

5.1.2 Setup

The study was carried out in a three-electrode cell. The reference electrode was a SCE. The auxiliary electrode was initially a stainless steel mesh but was replaced by graphite rods of at least two times the surface area of the exposed surface area of the working electrode, as is prescribed in ASTM G61 [64]. The results presented were attained with the graphite rod as auxiliary electrode. The working electrode was the specimen as described above.

A variety of standard corrosion cells, to position the electrodes and to set up the polarization test, are on the market. These are generally rather advanced to enable oxygen free corrosion tests. The cells that were available in the lab did not facilitate mixing with a stir bar. Therefore, a self-made corrosion cell was eventually used that consisted of an acrylic container with an electrode holder mounted on the top to ensure fixed distance between the electrodes. A schematization of the cell is given in Figure 20 and Appendix E.

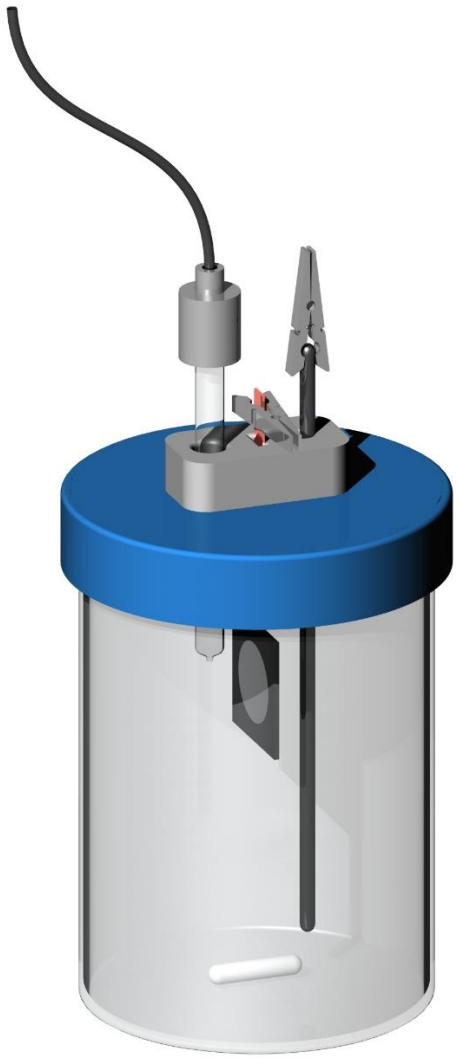

Figure 21: Corrosion cell set-up, assembled view without water.

5.1.3 Test conditions

The electrolyte was SCW either without inhibitor as base case, or with an inhibitor mixed at a specific concentration. The same type of inhibitors were used as in described in Section 2.2.4. The experiments were performed at least three times with the following type of solutions:

- Blanc: only SCW;
- NT100: SCW with 400 ppm NT containing 100% of the original phosphorus concentration;
- NT50: SCW with 400 ppm NT containing 50% of the original phosphorus concentration;
- NT0: SCW with 400 ppm NT containing 0% of the original phosphorus concentration;
- Si200: SCW with 200 ppm SiO_2 dosed as $Na_2SiO_3 \cdot 5H_2O$.
- Si100: SCW with 100 ppm SiO_2 dosed as $Na_2SiO_3 \cdot 5H_2O$.

The prepared specimens were immersed in a constantly stirred volume of 210 mL of one of the solutions, and hung vertically 1 cm under the free surface of the solution for a total of 6 days at room temperature. The 6 days of immersion were based on OCP measurements discussed in the results of the next section. After these 6 days, the OCP of the electrochemical cell was measured for at least 10 minutes. Consecutively, a CPP test was performed based on ASTM G61[64].

The applied potential of the CPP test started at -20mV vs. OCP, and increased in the more noble direction with a constant potential scan rate of 1.2 V/h. The scanning direction was reversed at the preset threshold current of 100 mA. This threshold current is one decade greater than the current recorded at the breakdown point. When this condition was not met, the scanning direction was reversed at the preset potential of 1.1 V. The reversed scan was stopped when the original OCP value was reached again.

The OCP and CPP tests were carried out on potentiostats of multiple brands due to practical reasons, although a single potentiostat was preferred for repeatability. The first potentiostat was a Solartron 1287 potentiostat/galvanostat that was connected to Solartron 1281 mulitplexer. The second one was a Solarton 1286 without a connection to a multiplexer. The third potentiostat was a Autolab PGSTAT302N and the fourth was a Biologic SP-200.

5.1.4 Surface analyses

Post-test visual examinations of the surface were carried out to evaluate the type of corrosion, the location of the corrosion and the dimensions of the eventual pits. This was done by simple photographs and by inspection with a Keyence Digital Microscope with a vh-z100r/w/t Wide-range Zoom lens (100-1000X). The SEM/EDS analysis were carried out using the JSM-IT100 from JEOL at high vacuum and the acceleration of the electron beam was 20.0 kV. The samples were mounted to the specimens stage with conductive adhesive to prevent the accumulation of electrostatic charge. The XRD analysis were carried out with a D8 Advance diffractometer from Bruker using Cu K-α X-ray energy.

5.2 Results and Discussion

5.2.1 OCP measurements

The duration of the specimen immersion, before a CPP was carried out, was based on OCP measurements with the Solartron 1287 in the solutions Blanc, NT0 and Si200. OCP measurements of eight days indicated a trend that confirmed the expected passivation development. No distinct difference in the trend was observed between the different solutions. The change rate of the OCP decreased the most during the first 36 hours. In a few cases, a drop in the OCP was measured followed by repassivation. This occurred generally during the first two days. Based on the time for the passivation to develop and the likelihood of a drop in the OCP during the first few days of immersion, a low OCP change rate was expected at 6 days of immersion. Additional measurements over a period of 6 days were executed to confirm this. Figure 22 provides an example of the OCP development measured with the Autolab PGSTAT302N. The trend could be described by a natural logarithm.

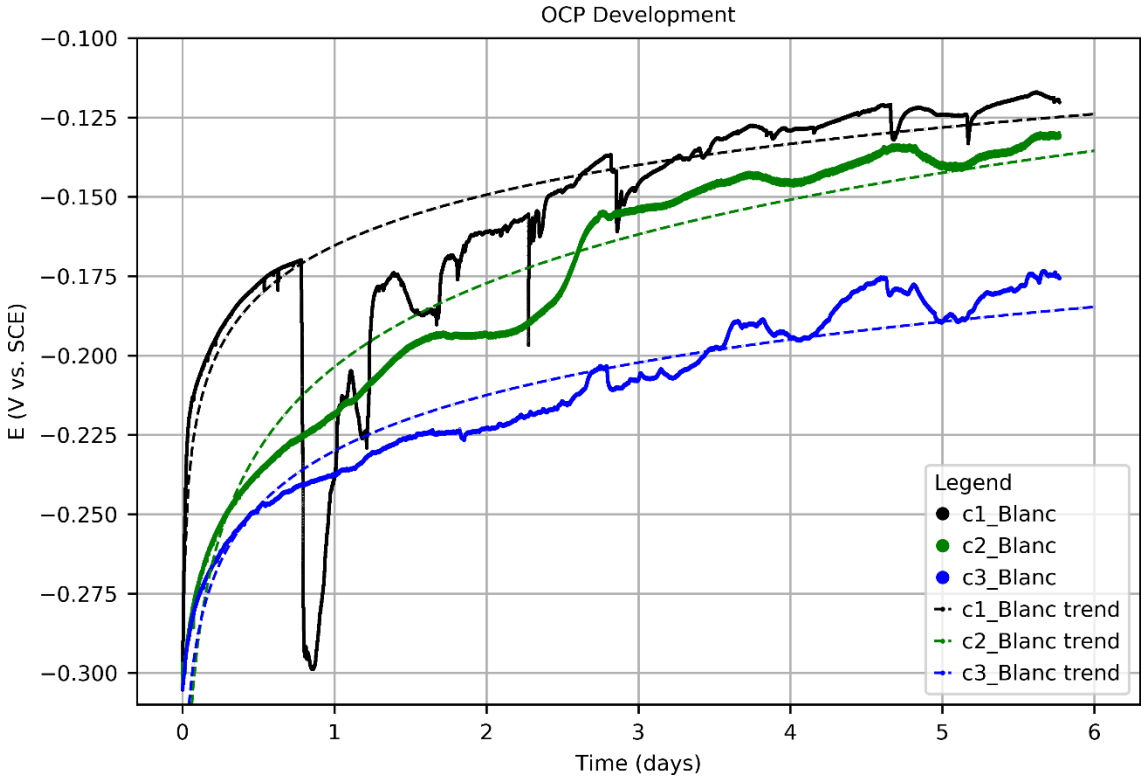

Figure 22: OCP Development of mild steel immersed in SCW.

Although the OCP values at the moment of immersion deviated from each other with approximately 10 mV, the final OCP values after 6 days show a larger deviation. The OCP values of all the samples that showed passivation behavior, have been summarized in Figure 23. The average OCP values of all solutions are within each other's range. So the inhibitors do not have a significant influence on the final OCP value.

The standards and literature often recommend and use a stabilization period of one hour or a maximum change rate, such as 3 mV/min as recommended by ASTM F2129 [66]. The specimens reached this maximum change rate within an hour. However, the specimens would not have had enough time to form a passivating layer on the surface before the CPP tests. CPP test that would only test the inhibition efficiency of inhibitors, and not in combination with the natural passivation of the metal sample, would require one hour of stabilization.

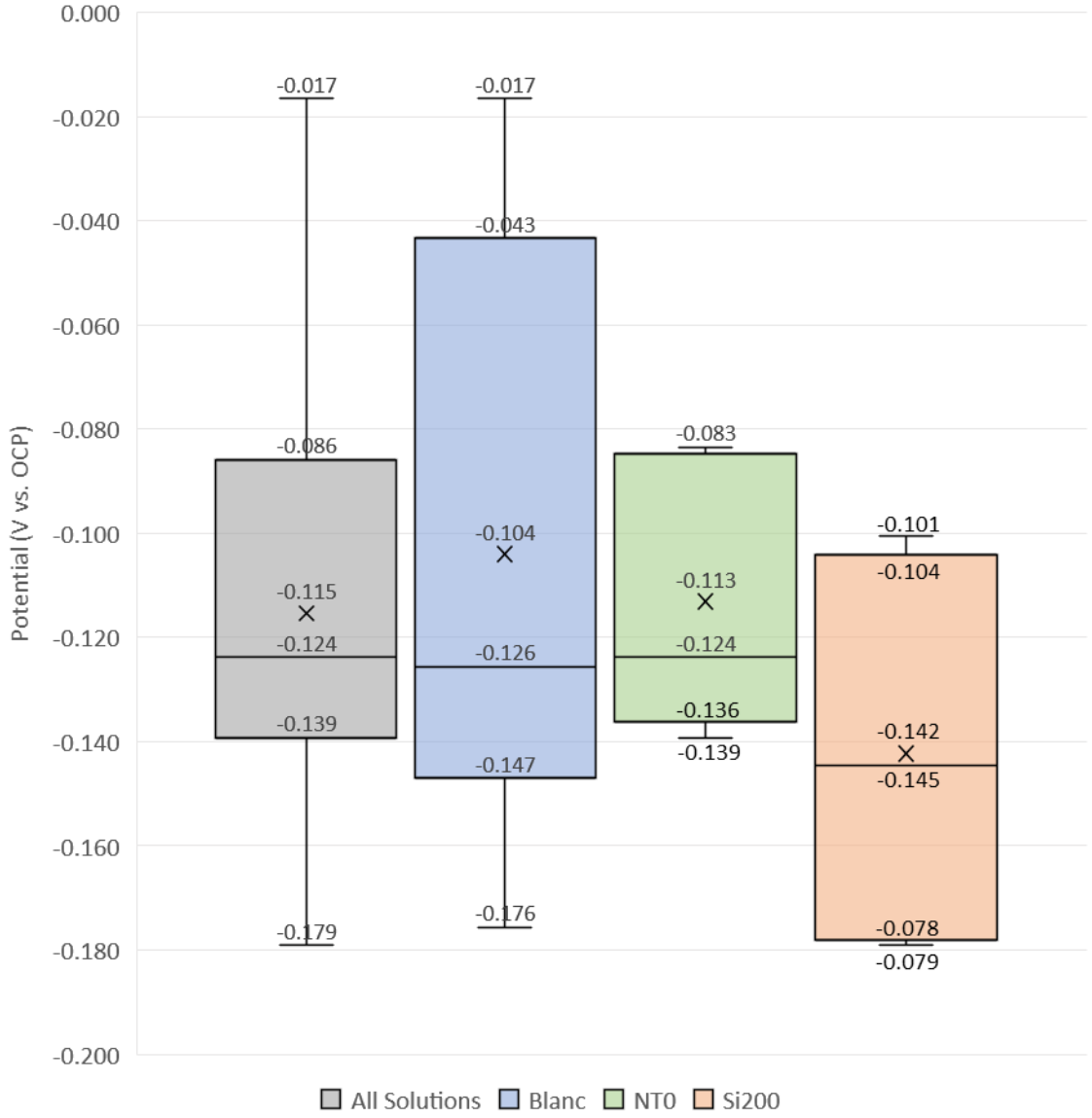

Figure 23: Final OCP values after 6 days of immersion in different solutions.

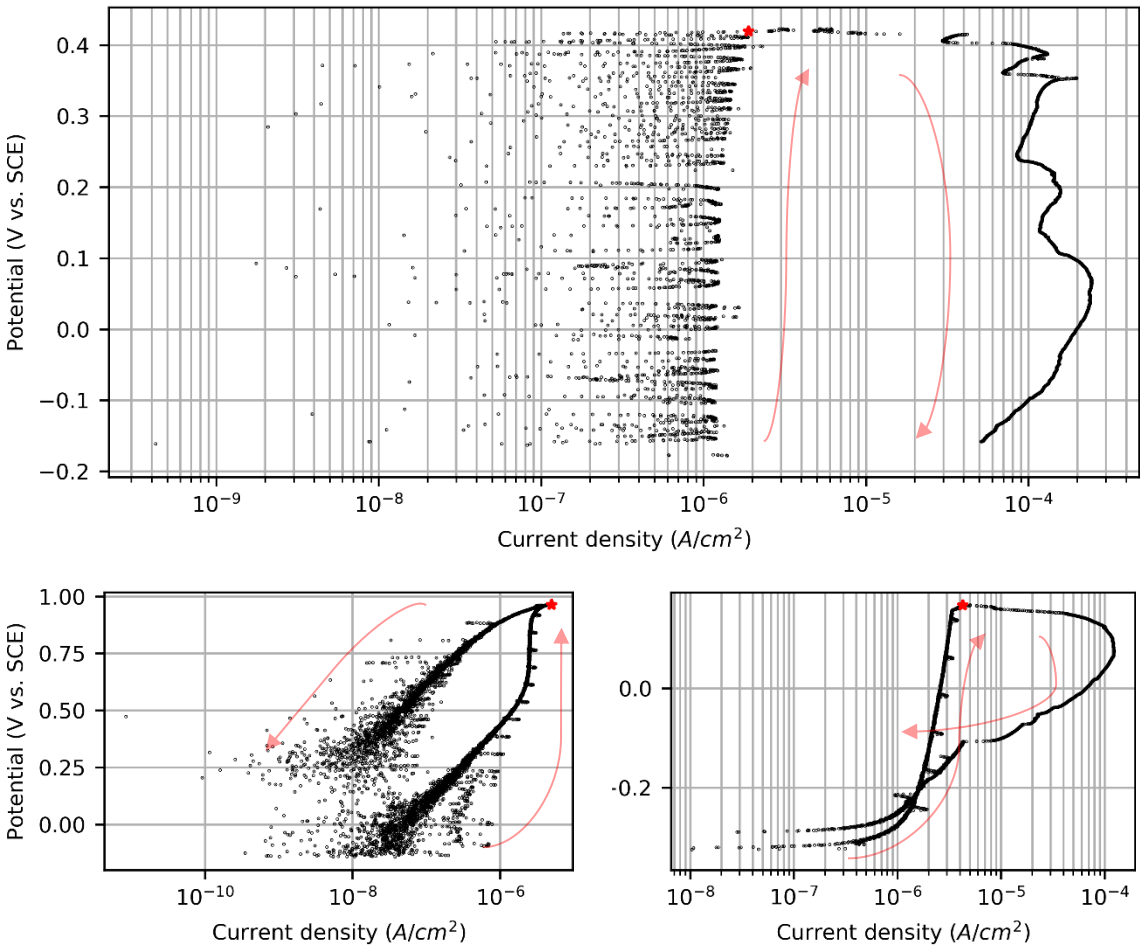

Figure 24: Three types of CPP curves: a) Passive behavior with breakdown of passivity; b) Active behavior followed by passive behavior and breakdown of passivity; c) Passive behavior without breakdown of passivity.

5.2.2 CPP measurements

The CPP measurements that followed the OCP measurements showed three type of polarization curves, as shown in Figure 24. Figure 24.a shows a polarization curve that is characterized by a vertical upward branch. Specimens that are sufficiently passivated start in the passivity domain and show this type of polarization behavior. Figure 24.b shows an steep increase of the current density at the beginning of the polarization scan, which can be related to specimens that are not completely passivated and which therefore start in the active domain. The distinct feature of Figure 24.c is the reversed branch that developed on the left side of the upward branch. This behavior is related to specimens where localized corrosion followed by breakdown of the passivity did not occur. At high potentials, the oxygen evolution potential can be reached, resulting in the oxidation of H_2O instead of the oxidation of the metal surface and therefore no breakdown of the passivity.

Active behavior, as in Figure 24.c, was often predicted before the CPP test. A small inhomogeneity at the interface of the polyester tape and the free metal surface that was spotted with close visual inspection with the naked eye, was an indication for active behavior. This was the case for 2 out of 27 specimens. CPP tests confirmed these observations. Due to practical problems with the potentiostats, the results obtained on the solutions NT100, NT50 and Si100 were not representative and are not further discussed.

Most specimens showed the behavior of Figure 24.a, where the initiation and propagation of localized corrosion occurred at potentials more electronegative than the oxygen evolution potential. An overview of the CPP results for the solutions Blanc, NT0 and Si200 is given in Figure 25. All upward anodic polarization scans showed similar slopes and metastability. The Blanc specimens showed distinct pit initiations and repassivations, which were less distinct for NT0 and Si200. The reversed branch of three solutions is clearly different, although none exhibited a protection potential. The Blanc CPP tests showed a jagged branch, which indicates unsuccessful attempts for repassivation and unstable pits, and followed an almost vertical path without decreasing in current density. The NT0 and Si200 tests did not have a jagged reverse branch and did decrease in the current density. The largest decrease in the current density is assigned to the solution NT0. From these results it was suggested that although the solutions with inhibitors have a lower breakdown potential, the inhibitors did have a positive effect on the environment at the pits and prevent pitting propagation.

Lower scan rates resulted in a more vertical upward branch and lower breakdown potentials because the system had more time to react and to stabilize. Higher scan rates can reduce the possibility of localized corrosion around gaskets and masks according to Scribner Associates [67]. The metastability can be the result of a too high scan rate. However, it is more likely that the metastability was the result of insufficient passivation. The insufficient passivation was probably located at the interface of the polyester tape and the free metal surface. Surface observations identified crevice corrosion and confirmed the presumed cause of the scattered branch. CPP tests with the same scan rate, but with specimens were active behavior initially dominated, did not result in a similar scattered result, as can be seen in Figure 24.

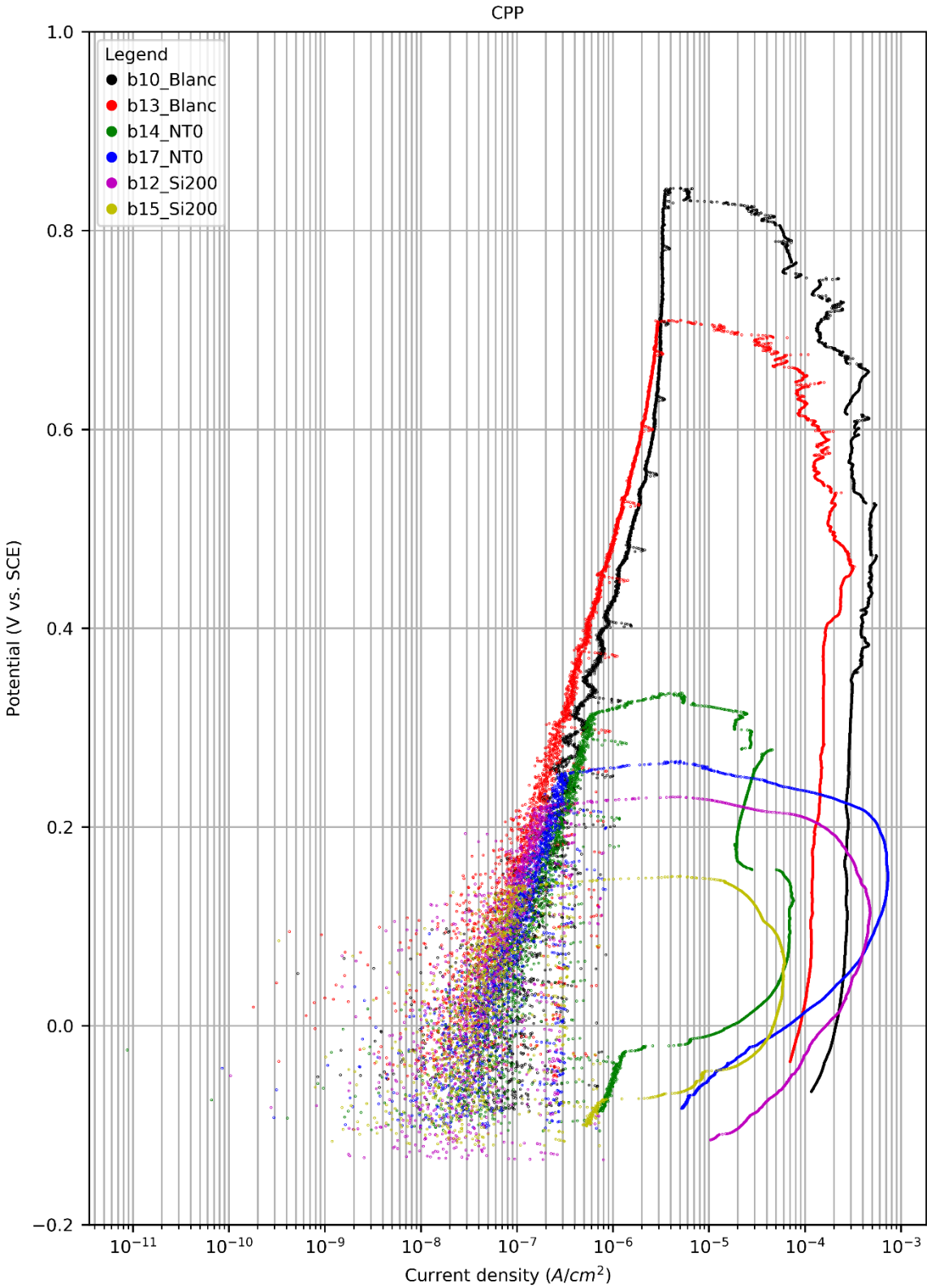

Figure 25: Overview of representative CPP curves.

The breakdown points of all CPP tests were extracted and summarized in Figure 26a. Some of these breakdown are not suitable for comparison due to a different scan rate, i.e. the points with higher breakdown potentials, or due to active behavior, i.e. the points with lower breakdown potentials. Figure 26b shows the breakdown points that were suitable for comparison, and demonstrate that the resistance to initiation and propagation of localized corrosion is highest for the Blanc solution and lowest for the Si200 solution, as in Figure 25. What became clear from Figure 26b is that a general linear relationship was distinguished of which the equation is given in the figure. The coefficient of determination (R^2) indicates a good fit of the line to the data points. The effect of the scan rate had most likely a larger influence on the breakdown points than the corrosion behavior itself. This was pointed out by comparing the slope of the linear fit with the slope of the anodic branch of the red curve in Figure 25, i.e. b13_Blanc, the values were 0.35 V/µA and 0.36 V/µA, respectively

Change of the pH during the CPP test could have affected the breakdown point. This becomes more likely when the test volume of the electrolyte is smaller. Measurements of the pH, EC and temperature before and after the polarization tests were not large enough to affected the breakdown point.

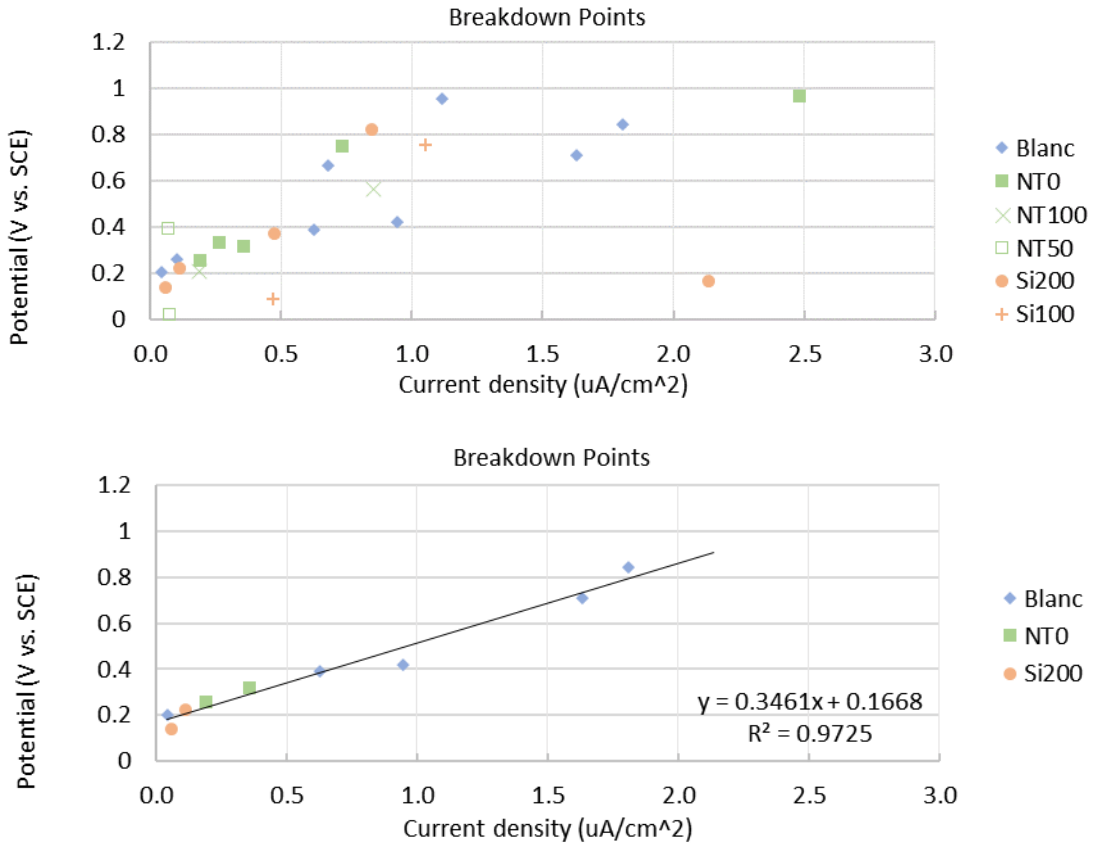

Figure 26: Overview of the breakdown points of the CPP tests with a) all CPP tests, and b) with only the representative CPP tests.

5.2.3 Surface analyses

Post-analysis by visual inspection before and after etching of the specimen surface confirmed that crevice corrosion took place at the interface of the polyester tape and the free metal surface, as is shown in Figure 27. 3D-microscopy was used to analyze the shape of the pits that were formed during the CPP tests. An example of such a 3D image is given in Figure 28. The maximum depth to average width ratio was calculated and presented for the three solutions in Figure 29. It appears that the presence of inhibitors resulted in more shallow pits, with the best results for Si200. This is in agreement with what was previously stated based on shape of the CPP curves, that the inhibitors reduced the corrosion propagation at the pit location.

Passivation of the metal surface was confirmed not only by OCP and CPP measurements, but also by XRD and SEM/EDX analysis. SEM/EDX analysis indicated iron oxides for the Blanc and NT0 solutions. Fe_2O_3 was identified on all samples that were immersed in the Blanc, NT0 and the SiO2 solutions, as is shown in the XRD results in Table 8 and Appendix H. No precipitated silica was found in the form of quarts. Amorphous silica scales cannot be detected by XRD. Other analysis techniques are required to assert the presence or absence of silica scale. SEM/EDS is such a method that should be able to detect silica scale. Some products at the edges of pits after CPP tests in Si200 solutions indicated the presence of silica, as is shown in Figure 31.b. However, the adsorbed layers were most likely affected by the removal of the specimens from the solution and by the introduction of the specimens in high vacuum.

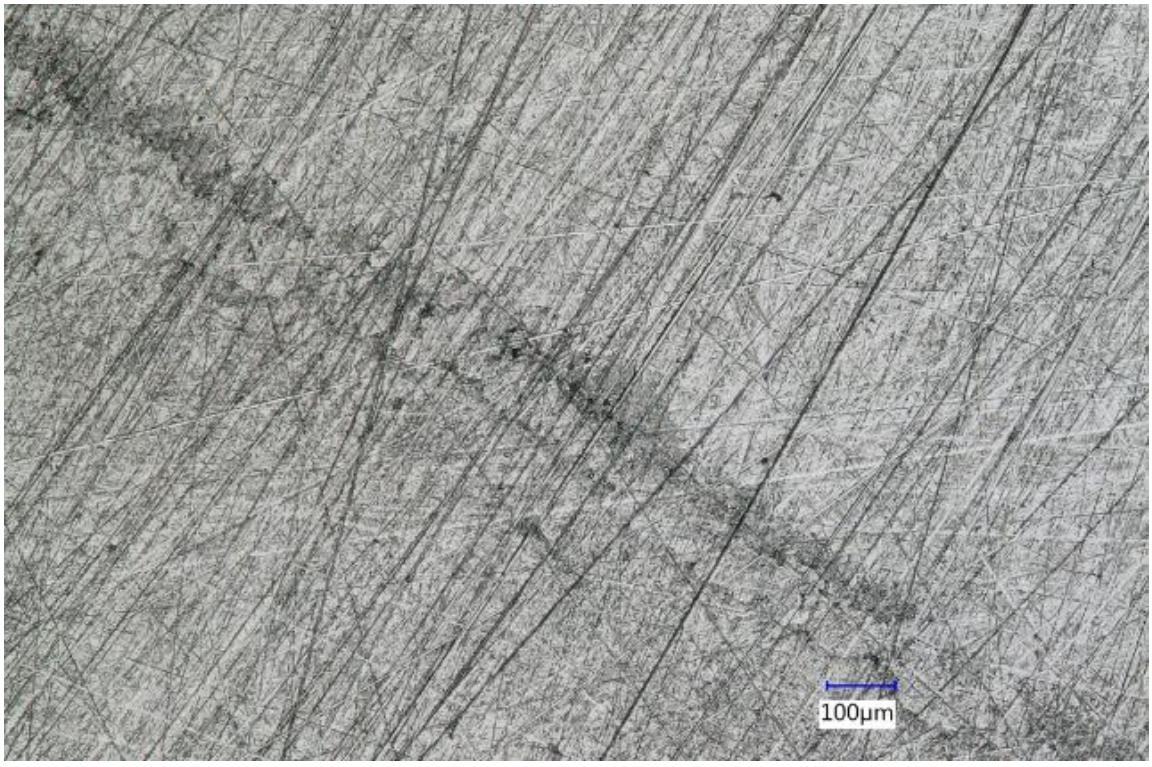

Figure 27: Digital microscopy image at 200x of crevice corrosion at the polyester interface.

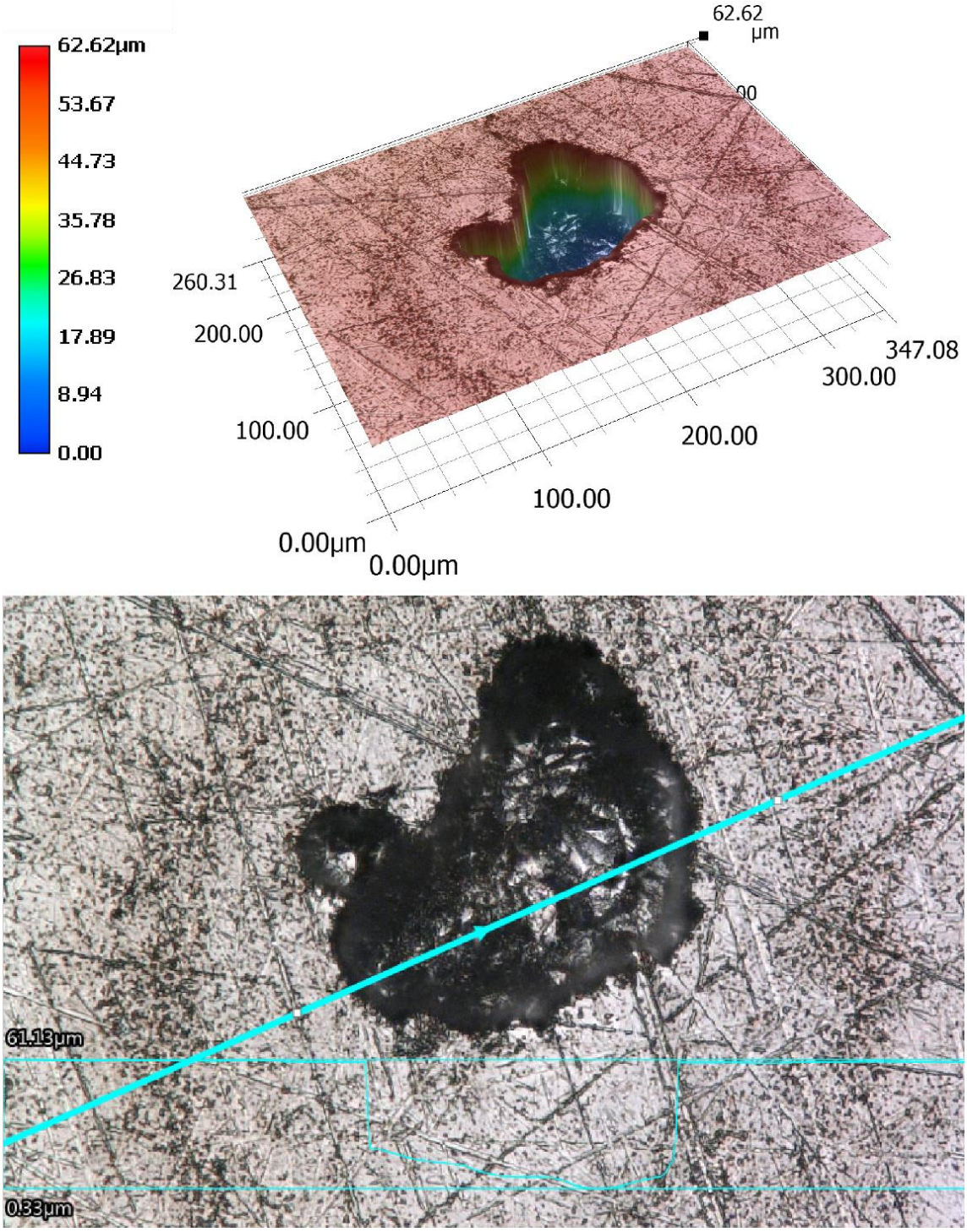

Figure 28: Digital microscopy images of a pit after a CPP test, a) 3D image, b) top view image with depth profile.

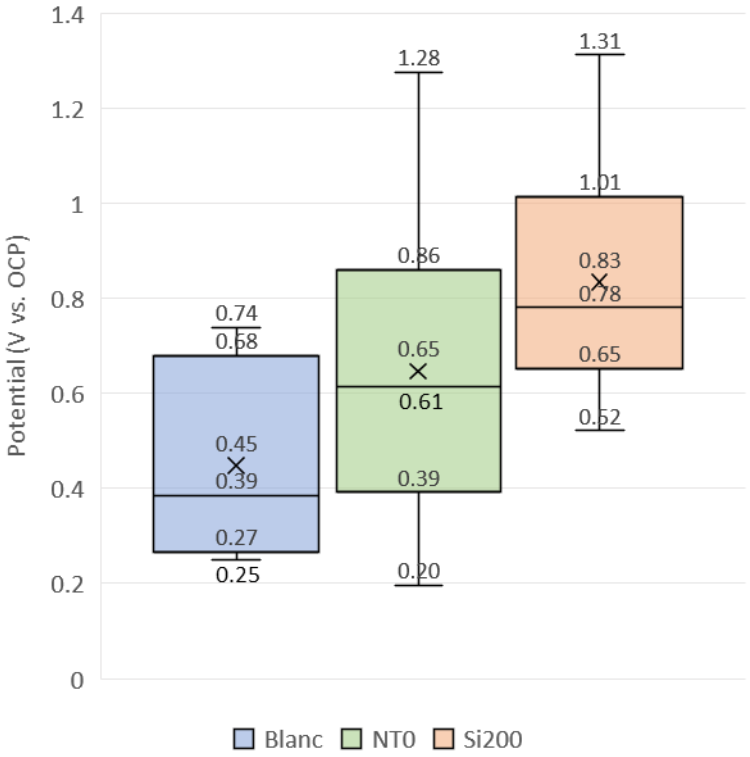

Figure 29: The maximum depth to average width ratio of pits after CPP tests.

Table 8: XRD results.

Sample	Compound	Compound
Blanc	Iron	Fe
	Iron oxide	Fe_2O_3
	Iron carbide	FeCx
NT0	Iron	Fe
	Iron oxide	Fe_2O_3
	Iron carbide	FeCx
Si2000	Iron	Fe
	Iron oxide	Fe_2O_3
	Iron carbide	FeCx

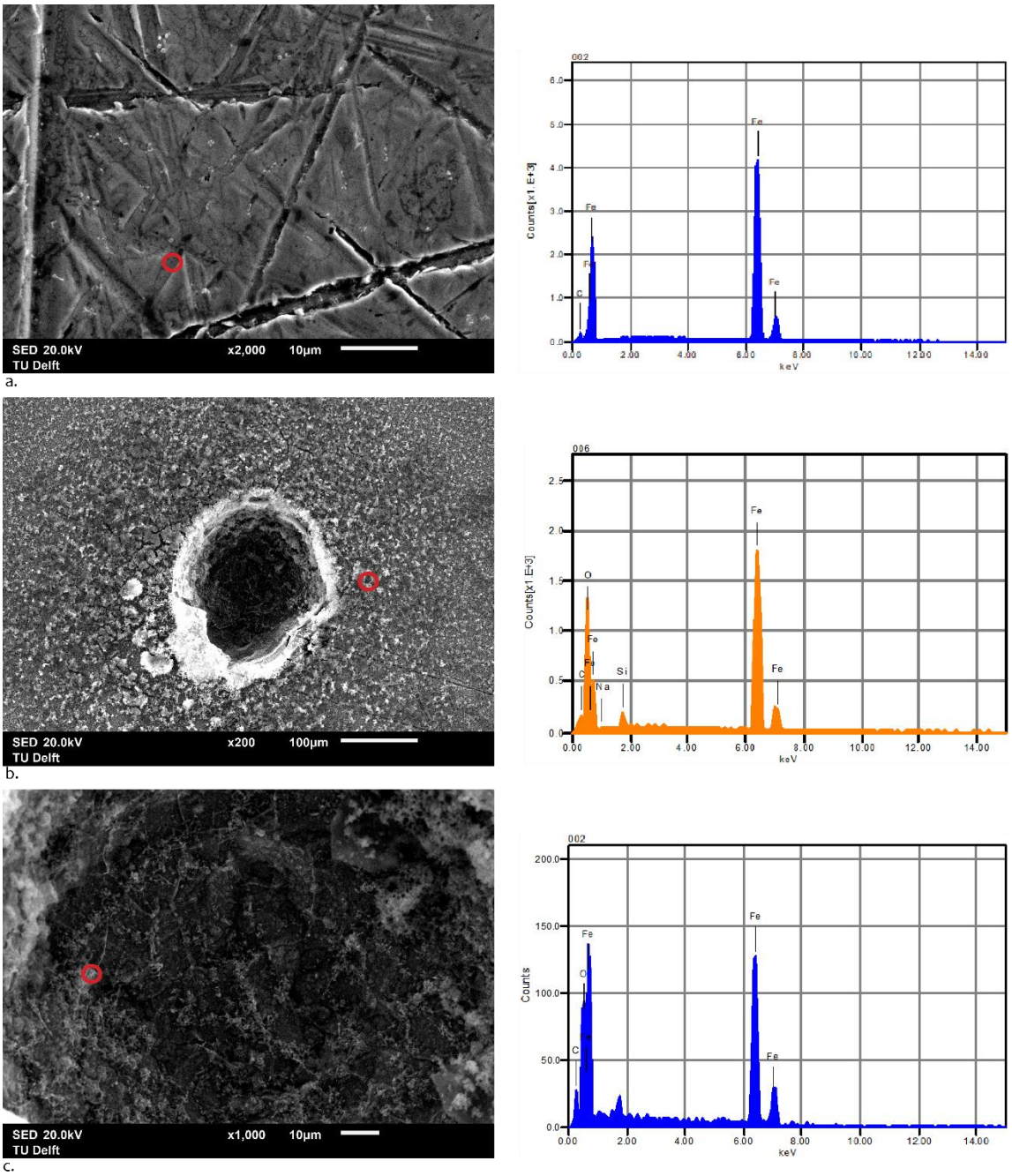

Figure 30: SEM/EDS results of a) uncorroded surface after CPP in Blanc solution, b) corrosion product outside a pit after CPP in Si200 solution, c) surface inside a pit after CPP in Si200 solution.

6 General discussion and Conclusions

The goal of this thesis was to gain understanding on the corrosion susceptibility of mild steel in SACW, to test the effect of different corrosion inhibitors on the corrosion susceptibility, and to explore phosphorus-free corrosion inhibitors for this type of cooling water. This was done through literature research, brief simulations in PHREEQC and lab experiments. Based on this information, answers to the research questions raised in Chapter 1.2 are provided in this chapter.

A. How can the corrosion behavior of mild steel in soft alkaline cooling water be evaluated?

First of all, the composition and quality parameters of SACW must be known and, just as importantly, the water must also be physically available to be used in experiments. Therefore, SCW was produced of which the composition and quality was based on the data of three surface water intake points in The Netherlands that are indirectly used for cooling water production. The concentrations of the ions in the surface water were increased to the desired COC. Simplifications were made by leaving out trace elements, organic carbon and iron. A natural pH of 9.1 was reached based on the carbonate equilibrium. The pH was increased by lowering the $NaHCO_3$ dosage and increasing the Na_2CO_3 dosage. The Ca^{2+} and Mg^{2+} concentrations that are normally present in surface water were completely exchanged for Na^+ for the composition of synthetic soft water, as if the CIEX had a 100% efficiency in removing the hardness. The calculations and the composition were validated using CBE calculations, PHREEQC simulations, pH and EC measurements and IC analysis.

The corrosion assessment techniques started off with desk studies related to corrosion indices and saturation indices in PHREEQC. Thereafter, mass loss tests and polarization experiments were carried out. At last, surface analyses were undertaken to verify the results obtained in the other experiments.

The corrosion indices that appeared to be most suitable for SACW have been evaluated. These turned out to be inappropriate for this kind of cooling water because they were based too much on empirical relationships for waters with their characteristics within a specific range.

PHREEQC simulations were used to check the SCW composition, whether it is suitable for the experiments and which type of scaling products could be expected. The scaling products that emerge from running the simulation can be evaluated for their benefits and disadvantages for the protection of the CWS.

A variety of lab experiments are possible to determine the corrosion rate. The most wide applied tests are mass loss tests. Mass loss tests in SCW can be carried out with different durations and multiple specimens in a setup of 2L jars to provide an estimate on the corrosion rate and corrosion type. Determination of the corrosion efficiency based on mass loss is only appropriate for specimens showing the same type of corrosion. Differentiation should be made between the inward and the outward facing side of the specimens.

OCP, PR and CPP tests are also suitable for testing the corrosion of mild steel and SCW is a suitable medium. These polarization tests can be carried out in simplified corrosion cells with 210 mL of SCW. OCP tests should run for several days if the formation and corrosion resistance of a passive layer is evaluated. Crevice corrosion can easily distort the measurements of passivated samples. In case only the performance of inhibitors is evaluated and not on the natural protection of the metal by an oxide, only one hour of stabilization is required before starting the CPP measurements. Not only CPP tests, but also Tafel plots can be determined form which the corrosion rate can be derived and the effect of the inhibitor on the anodic or cathodic curve. This report focused however on mild steel that was passivated by a naturally formed iron oxide layer. The creation of Tafel plots requires cathodic polarization which will remove the oxide layer. Therefore, the corrosion rate was not determined based on Tafel plots.

Visual surface analysis with the naked eye and digital microscopy with a magnification up to 1000x provided information on the surface morphology, i.e. the type of corrosion and the depth-width ratio of possible pits. The elemental composition found at the surface was identified with SEM/EDS. XRD is a useful method to identify the crystalline structure of oxide products and possible precipitates. Possible silica scale products were most likely amorphous, which makes XRD unsuitable for silica scale identification. The adsorbed layers were most likely affected by the removal of the specimens from the solution and by the introduction of the specimens in the high vacuum of the SEM/EDS. More advanced techniques, such as EIS and FTIR have not been evaluated for this type of water but are likely to provide more insight in the adsorbed layer and the surface characteristics of the specimen.

B. What is the effect of soft alkaline cooling water on the corrosion behavior of mild steel?

It was derived from the potential-pH diagram for iron in an aerated solution that mild steel would be naturally passivated by a protective oxide layer at pH 9.3. Two different types of specimens were used that had slightly different chemical composition but also different roughness. The specimens with the 1200-grit polish, confirmed the expectations based on the potential-pH diagram. The specimens with a four times higher roughness showed however uniform corrosion. The suggested reason for this is the inability of the specimen to form a homogeneous protective oxide layer on the surface due to the surface roughness.

The 1200-grit polished specimens showed an increase in potential over a period of six days similar to a natural logarithmic trend. This implicated the development of a passivating layer. Anodic potentiodynamic polarization, starting at -20mV vs. OCP, reaffirmed this. XRD measurements also confirmed the presence of protective Fe_2O_3.

The anodic branch of the CPP tests showed some pit initiations before actual propagation. At a scan rate of 0.6 V/h the breakdown potential of mild steel in SCW was 0.4 ± 0.02 V vs. SCE. The reversed branch indicated that the environment at the pits did not prevent further propagation, nor did the mild steel specimens repassivate in SCW.

C. How do different non-toxic corrosion inhibitors affect the corrosion behavior of mild steel in soft alkaline cooling water?

Two type of non-toxic inhibitors were used, namely NovoTraqua® and sodium silicate. The addition of NT0 and Si200 inhibited uniform corrosion but did not provide complete protection against localized corrosion in the mass loss tests. Si200 performed certainly the best as inhibitor. The inhibition efficiency of different inhibitor concentrations has to be tested though, because localized corrosion can be the result of too low inhibitor concentrations.

The inhibitors did not influence the OCP value after six days of immersion when compared to the OCP of the Blanc solution. The breakdown potential derived from the CPP tests was highest for the Blanc solution and lowest for the Si200 solution, which was against expectations. This is most likely due to a too high scan rate. Lower scan rates resulted in much lower breakdown potentials for the Blanc solution while the NT0 and Si200 solutions did not have a similar decrease in breakdown potential.

The CPP tests did not show considerable difference in the anodic upward branch for the specimens in different solutions. The reversed branch was however less jagged and showed attempt for repassivation for the inhibited solutions when compared to the Blanc solution. This was related to the positive effect the inhibitors had on the environment at the pits. The explanation was sought in the attraction of the negative dipoles of the inhibitors by the positively charged pits providing protection against aggressive ions. Without inhibitors, only aggressive ions like Cl^- and SO_4^{2-} would be attracted by the positive pit, resulting in pit propagation. The pits of the Si200 solution were most shallow relative to their width, and deepest for the Blanc solution. So the surface analyses confirmed what was derived from the CPP tests.

D. How do different concentrations of phosphorus in the corrosion inhibitor affect the corrosion behavior of mild steel in soft alkaline cooling water?

Literature review described that phosphonates catalyze the oxidation of ferrous hydroxide to gamma iron oxide. Based on this it was likely that the oxide layer at the mild steel surface would be less protective at lower dosages of phosphonates. So more localized corrosion and lower breakdown potentials were expected. Tests with different concentrations of phosphonates in the NovoTraqua® product were not successful due to practical reasons. This research question is therefore left unanswered and recommendations are provided in the next chapter.

7 Recommendations

The results presented in this report may contribute to the decision making and understanding of other (pilot scale) research projects that seek for alternative and more sustainable operation of current CWS. The research also resulted in new questions and recommendations for further research which are discussed below.

The immersion setup should be optimized to allow for automatic temperature regulation of the water inside the jugs and to allow for automatic inhibitor dosage. This provides the opportunity to perform corrosion tests at temperatures that generally occur in CWS. It would also provide the opportunity to test the inhibitor performance at different temperatures. Inhibitors that rely on physical adsorption are expected to have a lower inhibition efficiency at higher temperatures. So relative inhibition efficiencies at room temperature may not present the same relative inhibition efficiencies at higher temperatures.

The last research question was not answered, however it is still worthwhile to research the effect of different inhibitor concentrations and different phosphorus concentrations within the inhibitors. This can result in knowledge on the adsorption strength of an inhibitor. The corrosion data would have to be fitted to various adsorption isotherms, for example the Langmuir and Frumkin isotherms. The best fit would provide information on the thermodynamics of the inhibitor adsorption.

Similar tests can be conducted as presented in this report. The dynamic polarization tests would require only 1 hour stabilization period to test the different inhibitor and phosphorus concentrations. It is recommended to establish complete Tafel plots to evaluate the effect of the inhibitor on the cathodic and anodic curve and to determine the corrosion rate. Crevice corrosion should not influence the measurements. Coating the specimen instead of polyester tape, rubber O-ring or PTFE mask is recommended.

This study made use of different analytical techniques to identify surface morphology, deposits and scales. The used techniques were optical microscopy, SEM/EDS, and XRD. More advanced techniques such as Fourier Transform Infrared Spectroscopy (FTIR) and Electrochemical Impedance Spectroscopy (EIS) are recommended to obtain better understanding of the adsorbed layers and the inhibition mechanis. FTIR can be a useful method for obtaining information on the functional groups, and for the detection of vibrational frequencies of the bonds that are linked to specific chemical species. It is particularly suitable for the identification of organic substances in deposits. Additionally, FTIR provides the opportunity to follow surface layer growth. [68] EIS provides information on the adsorbed layer and the interaction with the metal surface by modelling the corrosion cell as an electrical circuit with several electrical elements.

This research focused on the corrosion behavior of mild steel in SACW. The high pH and phosphorus limited conditions most likely affect microbiological growth in the CWS. So robust and reliable operation of a CWS with this type of water does not only require revision of the corrosion inhibitors, but also revision of the need for dispersants and biocides. This research made use of SCW with a composition of a COC of 10. It is recommended to run experiments at different COC to determine the range of the eventual conditioning program and to evaluate of further reduction of water intake and chemicals can be accomplished.

8 Bibliography

[1] D.J. Flynn, The Nalco Water Handbook, third ed., McGraw-Hill Professional, New York, 2009.

[2] P.A. Saini, I.H. Farooqi, A. Hussain, M.A. Quraishi, Study of low cost eco-friendly compounds as corrosion inhibitors for cooling systems, Anti-Corrosion Methods Mater. 46 (1999) 328–335. doi:10.1108/00035599910295508.

[3] I.T. Miettinen, T. Vartiainen, P.J. Martikainen, Phosphorus and bacterial growth in drinking water., Appl. Environ. Microbiol. 63 (1997).

[4] BiOPhree, (n.d.). http://www.aquacare.nl/nl/ (accessed July 6, 2018).

[5] F. Oesterholt, H. Huiting, N. Koeman-Stein, L. Paping, Cooling water conditioning in the future, 2016. https://www.tkiwatertechnologie.nl/wp-content/uploads/2015/08/KWR-2016.069-Cooling-Water-Conditioning-in-the-Future-V3.0_final_public.pdf (accessed March 23, 2017).

[6] P.R. Roberge, P.E.N. York, C. San, F. Lisbon, L. Madrid, M. City, M.N. Delhi, S. Juan, Corrosion Engineering : Principles and Practice, (2008). doi:10.1036/0071482431.

[7] J.E. Singley, The search for a corrosion index, J. Am. Water Works Assoc. (1981) 579–582.

[8] W.F. Langelier, THE ANALYTICAL CONTROL OF ANTI-CORROSION WATER TREATMENT, J. Am. Water Works Assoc. 28 (1936) 1500–1521. http://www.jstor.org/stable/41226418.

[9] R.V. Skold, T.E. Larson, Measurement of the instantaneous corrosion rate by means of polarization data, Corrosion. 13 (1957) 69–72.

[10] T.M. Riddick, The mechanism of corrosion of water pipes, Water Sew. Work. 91 (1944).

[11] R. Touir, M. Cenoui, M. El Bakri, M. Ebn Touhami, Sodium gluconate as corrosion and scale inhibitor of ordinary steel in simulated cooling water, Corros. Sci. 50 (2008) 1530–1537. doi:10.1016/J.CORSCI.2008.02.011.

[12] B. Zhang, C. He, X. Chen, Z. Tian, F. Li, The synergistic effect of polyamidoamine dendrimers and sodium silicate on the corrosion of carbon steel in soft water, Corros. Sci. 90 (2015) 585–596. doi:10.1016/J.CORSCI.2014.10.054.

[13] J. Marín-Cruz, R. Cabrera-Sierra, M.A. Pech-Canul, I. González, EIS study on corrosion and scale processes and their inhibition in cooling system media, Electrochim. Acta. 51 (2006) 1847–1854. doi:10.1016/J.ELECTACTA.2005.02.104.

[14] D.J. Choi, S.J. You, J.G. Kim, Development of an environmentally safe corrosion, scale, and microorganism inhibitor for open recirculating cooling systems, Mater. Sci. Eng. A. 335 (2002) 228–235. doi:10.1016/S0921-5093(01)01928-1.

[15] M. Saremi, C. Dehghanian, M.M. Sabet, The effect of molybdate concentration and hydrodynamic effect on mild steel corrosion inhibition in simulated cooling water, Corros. Sci. 48 (2006) 1404–1412. doi:10.1016/j.corsci.2005.06.009

[16] Y.W. Kim, J.G. Kim, D.J. Choi, Development of a blended corrosion, scale, and microorganism inhibitor for open recirculating cooling systems, Mater. Corros. 52 (2001) 697–704.

[17] M.A. Ahmed, Inhibition of mild steel corrosion in cooling systems by low-and non-toxic corrosion inhibitors, The University of Manchester, 2016. https://www.research.manchester.ac.uk/portal/files/60828940/FULL_TEXT.PDF (accessed April 6, 2018).

[18] J.P. Broomfield, Corrosion of steel in concrete: understanding, investigation and repair, CRC Press, 2003.

[19] M. Finšgar, J. Jackson, Application of corrosion inhibitors for steels in acidic media for the oil and gas industry: A review, Corros. Sci. 86 (2014) 17–41. doi:10.1016/j.corsci.2014.04.044.

[20] S. Nešic, N. Nešic´, Key issues related to modelling of internal corrosion of oil and gas pipelines-A review, (2007). doi:10.1016/j.corsci.2007.06.006.

[21] M. Pourbaix, Atlas of electrochemical equilibria in aqueous solutions, Pergamon Press, New York, 1966.

[22] M. Poubaix, Potential-pH diagrams and metallic corrosion, in: W.H. Ailor (Ed.), Handb. Corros. Test. Eval., John Wiley & Sons, New York, 1971: pp. 661–687.

[23] U.R. Evans, Evidence in favor of an electrochemical mechanism of corrosion, J. Inst. Met. 30 (1923) 265–267.

[24] U.R. Evans, Isolation of the Film Responsible for the Passivity of an Iron Anode in Acid Solution, Nature. 126 (1930) 130.

[25] J.E.O. Mayne, M.J. Pryor, The Mechanism of Inhibition of Corrosion of Iron by Chromic Acid and Potassium Chromate., J. Chem. Soc. (1949) 1831.

[26] J.E.O. Mayne, J.W. Menter, M.J. Pryor, The Mechanism of Inhibition of the Corrosion of Iron by Sodium Hydroxide Solution, J. Chem. Soc. (1950) 3229.

[27] M. Cohen, The passivity and breakdown of passivity on iron, Passiv. Met. Ed. by RP Frankenthal, J. Kurger, NJ Princieton, Electrochem. Soc. (1978) 521.

[28] H.-H. Strehblow, Passivity of Metals Studied by Surface Analytical Methods, a Review, Electrochim. Acta. 212 (2016) 630–648. doi:10.1016/j.electacta.2016.06.170.

[29] S. Haupt, H.-H. Strehblow, Corrosion, Layer Formation, and Oxide Reduction of Passive Iron in Alkaline Solution: A Combined Electrochemical and Surface Analytical Study (1986) 873–885.

[30] ASTM International, G046 - Standard Guide for Examination and Evaluation of Pitting Corrosion, ASTM Int. (2013). doi:10.1520/G0046-94R13.

[31] D.A. Jones, Principles and prevention of corrosion, 2nd ed., Prentice-Hall, 1996.

[32] R.A. Pisigan Jr, J.E. Singley, Influence of buffer capacity, chlorine residual, and flow rate on corrosion of mild steel and copper, J. Am. Water Works Assoc. (1987) 62–70.

[33] T.E. Larson, R.M. King, Corrosion by water at low flow velocity, Corrosion. 10 (1954) 110–114.

[34] T.E. Larson, R.V. Skold, Laboratory studies relating mineral quality of water to corrosion of steel and cast iron, Corrosion. 14 (1958) 43–46.

[35] T. Fujii, T. Kodama, H. Baba, Influence of Water Quality and Flow Conditions on Corrosion of Carbon Steel Pipes in Fresh Water, Corros. Eng. 31 (1982) 637–642.

[36] I. Matsushima, Carbon steel corrosion in freshwaters, in: R.W. Revie (Ed.), Uhlig's Corros. Handb., Third, John Wiley & Sons, Inc, 2011: pp. 589–607.

[37] V.S. Sastri, Corrosion inhibitors: principles and applications, John Wiley & Sons, 1998.

[38] H.H. Uhlig, Uhlig's corrosion handbook, Third, John Wiley & Sons, Hoboken, New Jersey, 2011.

[39] M. Prabakaran, K. Vadivu, S. Ramesh, V. Periasamy, Corrosion protection of mild steel by a new phosphonate inhibitor system in aqueous solution, Egypt. J. Pet. 23 (2014) 367–377. doi:10.1016/J.EJPE.2014.09.004.

[40] B. Zhang, C. He, X. Chen, Z. Tian, F. Li, The synergistic effect of polyamidoamine dendrimers and sodium silicate on the corrosion of carbon steel in soft water, Corros. Sci. 90 (2015) 585–596. doi:10.1016/j.corsci.2014.10.054.

[41] O. Lahodny-Šarc, L. Kaštelan, The influence of pH on the inhibition of corrosion of iron and mild steel by sodium silicate, Corros. Sci. 21 (1981) 265–271. doi:10.1016/0010-938X(81)90002-0.

[42] L. Lehrman, H.L. Shuldener, Action of Sodium Silicate as a Corrosion Inhibitor in Water Piping, Ind. Eng. Chem. 44 (1952) 1765–1769. doi:10.1021/ie50512a023.

[43] M. Stern, A.L. Geary, Electrochemical polarization I. A theoretical analysis of the shape of polarization curves, J. Electrochem. Soc. 104 (1957) 56–63.

[44] ASTM International, G031 - Standard guide for laboratory immersion corrosion testing of metals, ASTM Int. (2012) 1–10. doi:10.1520/G0031-12A.

[45] ASTM International, G003 - Conventions Applicable to Electrochemical Measurements in Corrosion Testing, ASTM Int. G3-14 (2014) 1–10. doi:10.1520/G0003-14.2.

[46] NEN, NVN6419:2008: Protocol for the preparation of synthetic laboratory samples for organic compounds in ground- and surface water, (2008).

[47] United Nations, Globally harmonized system of classification and labelling of chemicals (GHS), New York and Geneva, 2011. https://www.unece.org/fileadmin/DAM/trans/danger/publi/ghs/ghs_rev04/English/ST-SG-AC10-30-Rev4e.pdf (accessed June 18, 2017).

[48] ASTM International, D1141-98(2013) Standard Practice for the Preparation of Substitute Ocean Water 1, (2013). doi:10.1520/D1141-98R13.

[49] R.L. Malcolm, P. MacCarthy, Limitations in the use of commercial humic acids in water and soil research, Environ. Sci. Technol. 20 (1986) 904–911.

[50] R.L. Malcolm, Geochemistry of stream fulvic and humic substances, Humic Subst. Soil, Sediment, Water Geochemistry, Isol. Charact. (1985) 181–209.

[51] G.B. Alexander, W.M. Heston, R.K. Iler, THE SOLUBILITY OF AMORPHOUS SILICA IN WATER, (1954). https://pubs.acs.org/doi/pdf/10.1021/j150516a002 (accessed June 1, 2017).

[52] C.A.J. Appelo, SPECIFIC CONDUCTANCE: how to calculate, to use, and the pitfalls, (2010). http://www.hydrochemistry.eu/exmpls/sc.html (accessed August 19, 2017).

[53] P. Atkins, J. De Paula, Atkins' physical chemistry, New York. (2006) 77.

[54] David L. Parkhurst, C.A.J. Appelo, Description of Input and Examples for PHREEQC Version 3—A Computer Program for Speciation, Batch-Reaction, One-Dimensional Transport, and Inverse Geochemical Calculations, 2013. ftp://brrftp.cr.usgs.gov/pub/charlton/phreeqc/Phreeqc_3_2013_manual.pdf (accessed August 19, 2018).

[55] I. Safari, M. Hsieh, S. Chien, M.E. Walker, R.D. Vidic, D.A. Dzombak, J. Abbasian, Effect of CO2 stripping on pH in open-recirculating cooling water systems, Environ. Prog. Sustain. Energy. 33 (2014) 275–282.

[56] H.S. Harned, R. Davis Jr, The ionization constant of carbonic acid in water and the solubility of carbon dioxide in water and aqueous salt solutions from 0 to 50, J. Am. Chem. Soc. 65 (1943) 2030–2037.

[57] H.S. Harned, S.R. Scholes Jr, The ionization constant of HCO3-from 0 to 50, J. Am. Chem. Soc. 63 (1941) 1706–1709.

[58] D.L. Gallup, P. von Hirtz, Control of Silica-Based Scales in Cooling and Geothermal Systems, in: Miner. Scales Depos. - Sci. Technol. Approaches, 2015: pp. 573–582.

[59] J.R. Davis, Corrosion: Understanding the basics, ASM International, 2000.

[60] ASTM International, G001 - Standard Practice for Preparing , Cleaning , and Evaluating Corrosion Test, ASTM Int. 90 (2011) 1–9. doi:10.1520/G0001-03R11.2.

[61] ASTM International, G005 - Standard Reference Test Method for Making Potentiodynamic Anodic Polarization Measurements, ASTM Int. (2014) 1–9. doi:10.1520/G0005-14.2.

[62] 3M België N.V. & 3M Nederland B.V., Productcatalogus tapes - tape oplossingen voor de industrie, (2010) 164. http://solutions.3mnederland.nl/3MContentRetrievalAPI/BlobServlet?lmd=1384938762000&locale=nl_NL&assetType=MMM_Image&assetId=1319209837063&blobAttribute=ImageFile (accessed May 6, 2018).

[63] ASTM International, D2688-Standard Test Method for Corrosivity of Water in the Absence of Heat Transfer (Weight Loss Method) 1, (2015). doi:10.1520/D2688-15E01.

[64] ASTM International, G061 - Standard Test Method for Conducting Cyclic Potentiodynamic Polarization Measurements for Localized Corrosion Susceptibility of Iron-, Nickel-, or Cobalt-Based Alloys 1, (2014). doi:10.1520/G0061-86R14.

[65] ASTM International, F746 Standard Test Method for Pitting or Crevice Corrosion of Metallic Surgical Implant Materials, (2014). doi:10.1520/F0746-04R14.

[66] ASTM F2129, F2129 Standard Test Method for Conducting Cyclic Potentiodynamic Polarization Measurements to Determine the Corrosion Susceptibility of Small Implant Devices, (2017). doi:10.1520/F2129-17B.

[67] Scribner, CView Manual, (1996).

[68] C.P. East, T.L. Schiller, C.M. Fellows, W.O.S. Doherty, Analytical Techniques to Characterize Scales and Deposits, in: Miner. Scales Depos. Sci. Technol. Approaches, 2015: pp. 681–700.

9 Abbreviations

AE	auxiliary electrode
ASTM	American Society for Testing and Materials
CBE	charge balance error
CIEX	cation exchange
COC	cycles of concentration
CPP	cyclic potentiodynamic anodic polarization
CWS	cooling water system
EC	electrical conductivity
EDS	energy dispersive spectroscopy
EIS	electrochemical impedance spectroscopy
FTIR	Fourier transform infrared spectroscopy
HTI	holding time index
IEX	ion exchange
KWR	KWR Watercycle Research Institute
NT	NovoTraqua®
OCP	open circuit potential
ORCWS	open recirculating cooling water system

Appendix A – HumVi production and composition

Vitens N.V. is a drinking water company that uses groundwater to produce drinking water by the following consecutive treatment processes: vacuum degassing, plate aeration, rapid sand filtration, CO_2 removal, pellet softening, caustic soda dosage, another rapid sand filtration, and finally ion exchange for color removal. The ion exchange tank is regenerated with a 10% NaCl solution. The depleted regenerate stream contains ca. 4% salt solution and a high concentration of TOC. To reach a product with a high TOC concentration and low salt concentration, the regenerate stream is concentrated by dead-end nanofiltration, nanofiltration and diafiltration. The composition of the final product HumVi is summed up in Table 9. (P. Sjoerdsma, personal communication, August 30, 2017)

Table 9: Composition of HumVi, a product with concentrated humic substances (Vitens N.V.). (HS=humic substances, i.e. humic and fulvic acids; See end of document for other abbreviations.)

	Unit	Value		Unit	Value	Percentage of TOC
Colour	[mg PtCo/L]	456691	**TOC**	[mg/L]	7.56	100%
TOC	[mg/L]	101514	**DOC**	[mg/L]	6.92	91,5%
pH		8.33	**POC**	[mg/L]	0.63	8,3%
EC	[mS/cm]	36.7	**HOC**	[mg/L]	0.29	3,8%
dry matter	[g/L]	228				
Salt/NaCl	[%]	0.85	**HS**	[mg/L]	2.92	38,6%
UV	[1/cm]	353103	**BB**	[mg/L]	2.32	30,7%
NO_3^-	[mg/L]	450				
HCO_3^-	[mg/L]	38402	**LMW acids**	[mg/L]	7.56	100%
CO_3^{2-}	[mg/L]	1172	**LMW neutr**	[mg/L]	6.92	91,5%
PO_4^{3-}	[mg/L]	17				
SO_4^{2-}	[mg/L]					
Cl^-	[mg/L]	5150				
Si	[mg/L]	200				
Na^+	[mg/L]	34991				
K^+	[mg/L]	14.2				
Fe	[mg/L]	121				
Mn	[mg/L]	4.58				
Ca^{2+}	[mg/L]	57				
Mg^{2+}	[mg/L]	59				

Appendix B – PHREEQC input file

```
Database C:\phreeqc\database\phreeqc.dat

#Defining Solution 1
SOLUTION        1 Simulated hard surface water starting at COC1
units           mg/l
pH              8       CO2(g) -3.1
temp            20
Alkalinity 160  as HCO3

Na      32
K       8.0
#Ca     60      as Ca
Ca      150     as CaCO3
#Mg     8       as Mg
Mg      35      as CaCO3
Amm     .1
Fe(+3)  .1
Mn      0.01
S(6)    52      #SO4-2
N(+5)   13      #NO3-
P       .4      as PO4
Cl      46
F       .2
Br      .09
Si      2       as SiO2
END

#Defining Solution 2
SOLUTION        2 Simulated soft surface water starting at COC1
units           mg/l
pH              8       CO2(g) -3.1
temp            20
Alkalinity      160     as HCO3

Na      116
K       8.0
Ca      0
Mg      0
Amm     .1
Fe(+3)  .1
Mn      0
Cu(+2)  0
S(6)    52.0    #SO4-2
N(+5)   13.0    #NO3-
P       .4      as PO4
Cl      46.0
F       .2
Br      .09
Si      2       as SiO2
END

#Increasing the COC of Solution 1 at T=20oC
USE solution 1
REACTION_TEMPERATURE 20
```

```
EQUILIBRIUM_PHASES
CO2(g) -3.1
REACTION 1
H2O -1
52.733 moles in 53 steps #COC20

USER_GRAPH 1
-headings              CoC SI_Calcite SI_Dolomite SI_Sepiolite SI_Talc pH
-axis_titles           "COC" "SI" "pH"
-initial_solutions     false
-chart_title           "Impact of COC on SIs and pH of hard water at 20oC"
-plot_concentration_vs x
-axis_scale x_axis     1 20 2
-axis_scale y_axis     -5 15 5
-axis_scale sy_axis    8 9.5 0.5
-start
10 graph_x 1/SOLN_VOL
20 graph_y si("Calcite")
30 graph_y si("Dolomite")
40 graph_y si("Sepiolite")
50 graph_y si("Talc")
60 graph_sy -la("H+")
-end
END
USER_GRAPH 1
-detach
END

#Increasing the COC of Solution 2 at T=20oC
USE solution 2
REACTION_TEMPERATURE
20
EQUILIBRIUM_PHASES
CO2(g) -3.1
REACTION 1
H2O -1
52.733 moles in 53 steps #COC20
USER_GRAPH 2
-headings              CoC SI_Chalcedony SI_Quartz pH
-axis_titles           "COC" "SI" "pH"
-initial_solutions     false
-chart_title           "Impact of COC on SIs and pH of soft water at 20oC"
-plot_concentration_vs x
-axis_scale x_axis     1 20 2
-axis_scale y_axis     -1 1 0.2
-axis_scale sy_axis    8 9.5 0.5
-start
10 graph_x 1/SOLN_VOL
20 graph_y si("Chalcedony")
30 graph_y si("Quartz")
40 graph_sy -la("H+")
-end
END
USER_GRAPH 2
-detach
```

(B.M van Breukelen, personal communication, October 09, 2017)

Appendix C – 4 weeks immersion test setup

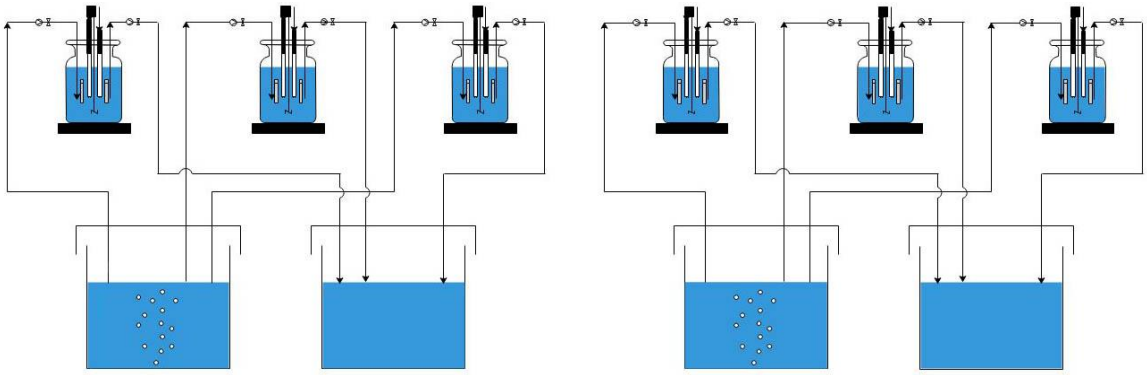

Figure 31: Schematization of the 4 weeks immersion tests setup.

Appendix D – Specimen composition and surface roughness

Table 10: Chemical composition of the specimens used in the Immersion tests and the Voltamettric tests.

Compound	Weight percent in Immersion tests	Weight percent of material in Voltamettric tests
C	0.08	0.087
M	0.330	0.375
P	0.011	0.013
S	0.009	0.013
Al	0.045	NA
Si	0.019	0.018
Fe	*remainder*	*remainder*

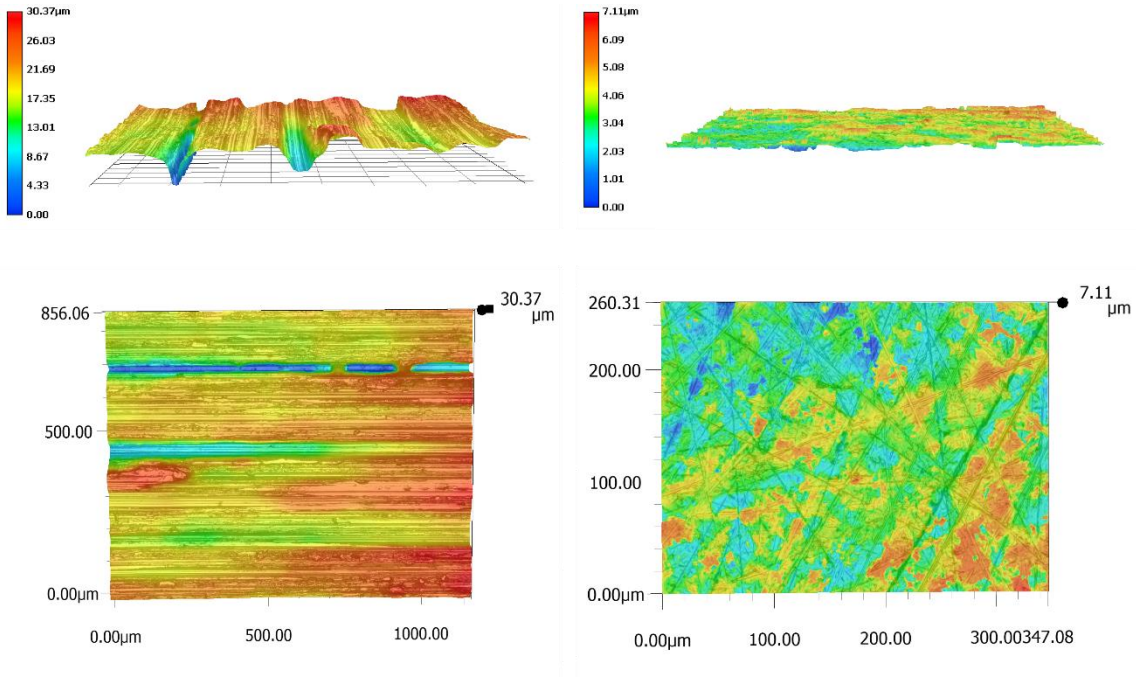

Figure 32: Surface roughness of Metal Samples Co coupon vs. self-made coupon.

Appendix E – Corrosion cell setup

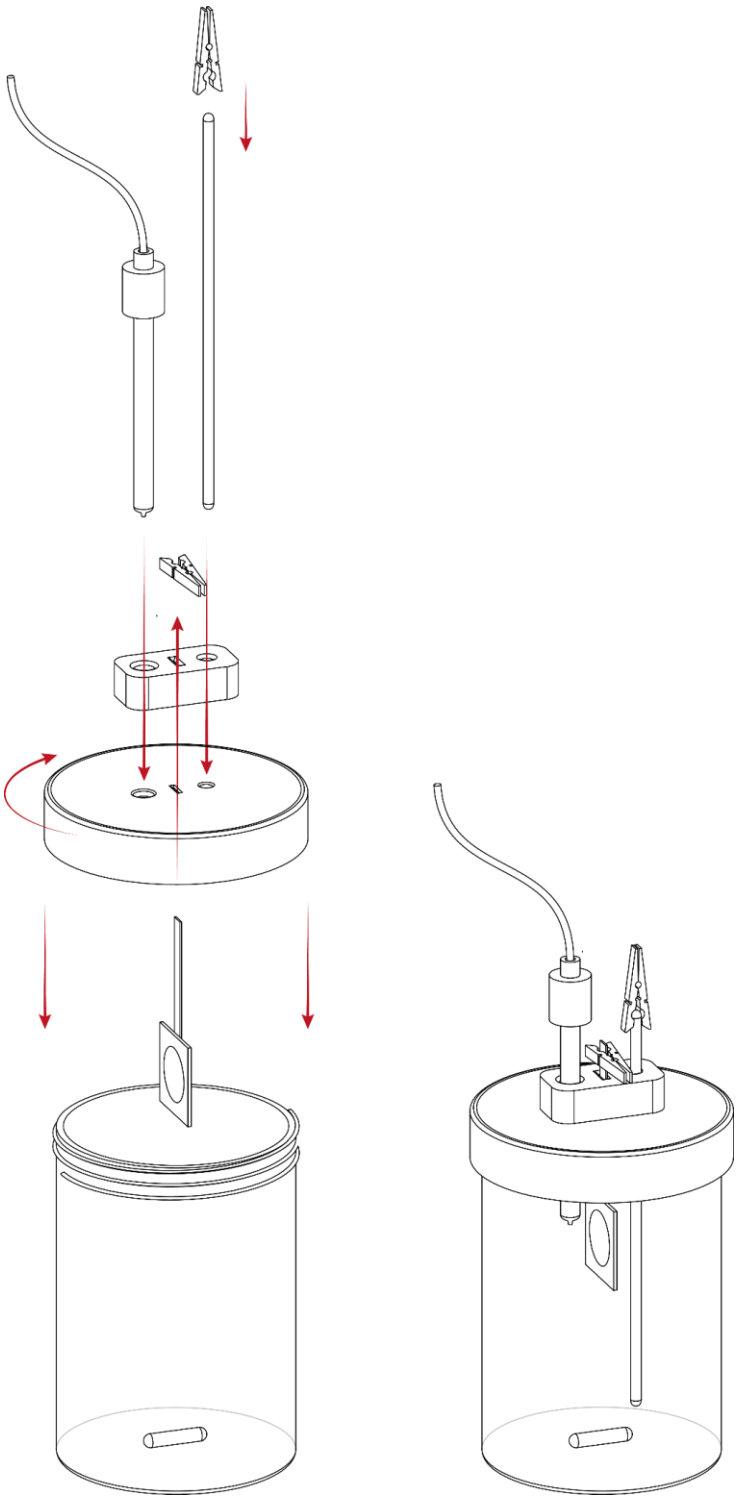

Figure 33: Line drawing of self-made corrosion cell

Appendix F – CPP test results

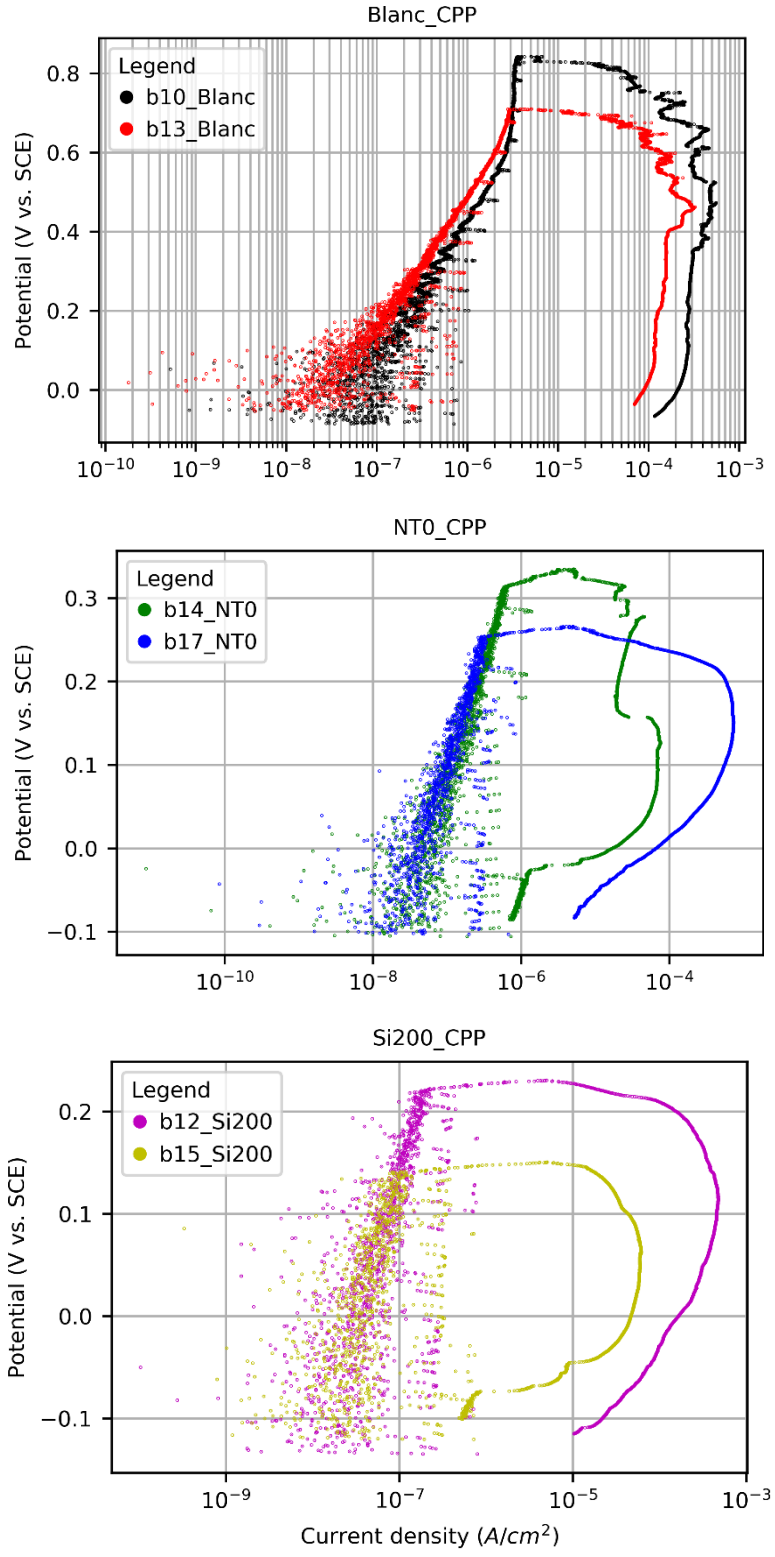

Figure 34: Overview of the CCP tests per solution type, with a) Blanc, b) NT0, and c) Si200.

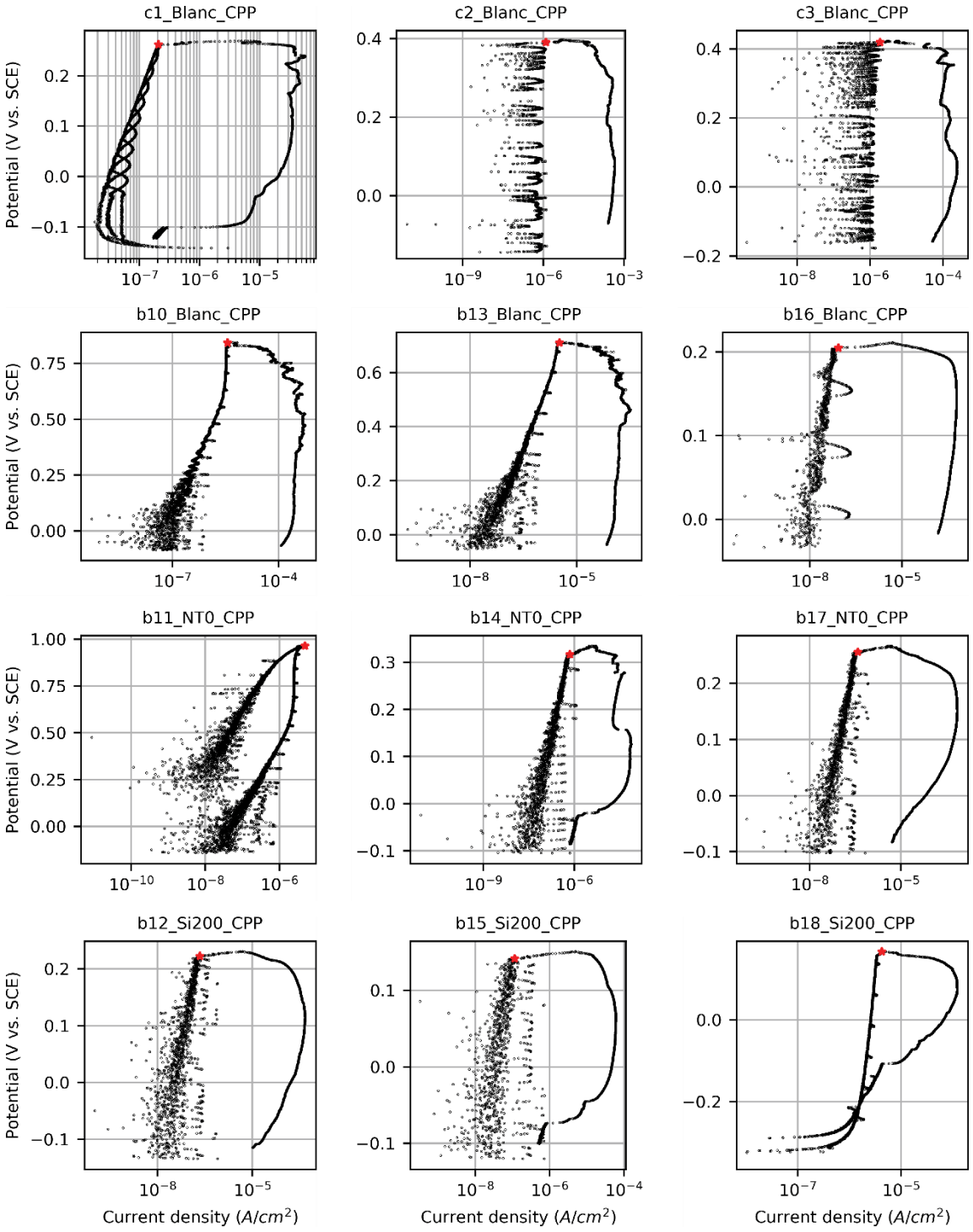

Figure 35: Overview of the CCP tests with the top two rows Blanc, third row NT0, and fourth row Si200.

Table 11: Overview of breakpoint or vertex indices, current densities and potentials.

Name	Index	Current Density (µA/cm2)	Potential (V vs. SCE)
a1_Blanc	918	0.680	0.666
a2_Blanc	1218	1.114	0.952
a3_NT0	992	0.734	0.746
a4_NT0	522	0.265	0.332
a5_Si200	614	0.474	0.372
a6_Si200	1122	0.848	0.823
b10_Blanc	3708	1.808	0.842
b11_NT0	4419	2.479	0.962
b12_Si200	1422	0.111	0.222
b13_Blanc	3054	1.631	0.709
b14_NT0	1685	0.357	0.316
b15_Si200	1043	0.057	0.141
b16_Blanc	963	0.043	0.204
b17_NT0	1427	0.193	0.255
b18_Si200	2025	2.136	0.166
c2_Blanc	3207	0.628	0.390
c3_Blanc	3582	0.944	0.419

Appendix G – Surface visualization after CPP tests

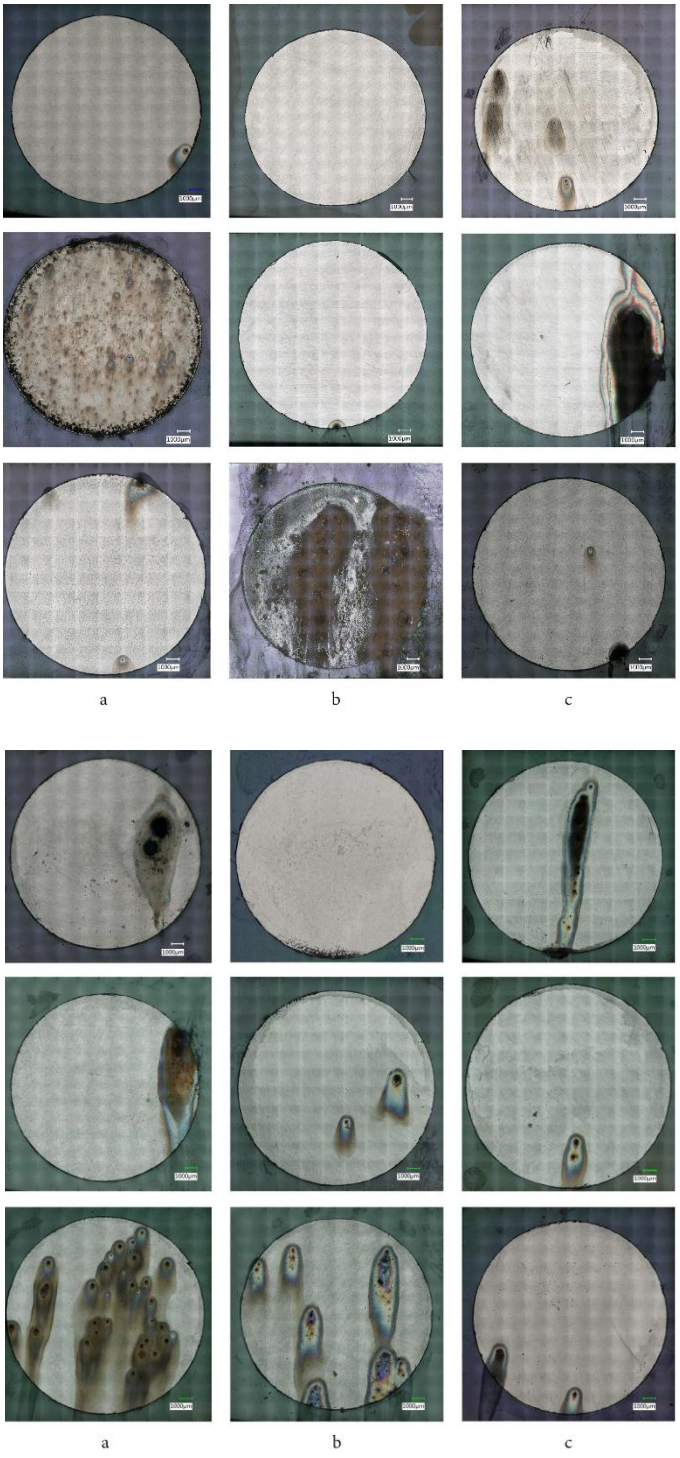

Figure 36: Overview of the surfaces after CCP tests per solution type, with column a) Blanc, column b) NT0, and column c) Si200.

Appendix H – XRD results

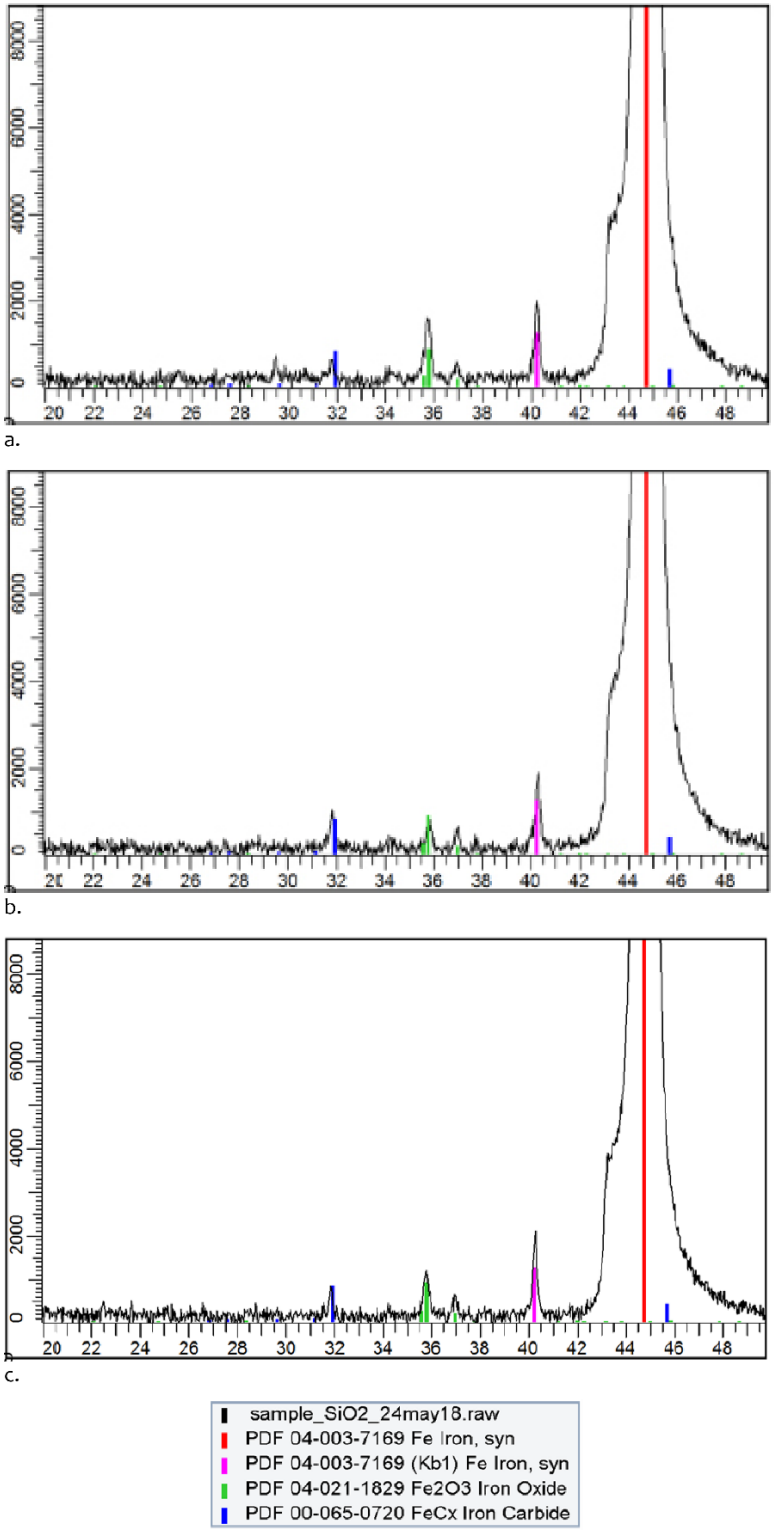

Figure 37: XRD measurements of mild steel coupons after immersion in a) Blanc, b) NT0 and c) Si200 solutions.